Critical behavior of three-dimensional Ising spin glass models

Martin Hasenbusch,[1] Andrea Pelissetto,[2] and Ettore Vicari[3]
[1]*Institut für Theoretische Physik, Universität Leipzig, Postfach 100 920, D-04009 Leipzig, Germany*
[2]*Dipartimento di Fisica dell'Università di Roma "La Sapienza" and INFN, I-00185 Roma, Italy*
[3]*Dipartimento di Fisica dell'Università di Pisa and INFN, I-56127 Pisa, Italy*
(Received 27 September 2008; published 17 December 2008)

We perform high-statistics Monte Carlo simulations of three-dimensional Ising spin glass models on cubic lattices of size L: the $\pm J$ (Edwards-Anderson) Ising model for two values of the disorder parameter p, $p=0.5$ and $p=0.7$ (up to $L=28$ and $L=20$, respectively), and the bond-diluted bimodal model for bond-occupation probability $p_b=0.45$ (up to $L=16$). The finite-size behavior of the quartic cumulants at the critical point allows us to check very accurately that these models belong to the same universality class. Moreover, it allows us to estimate the scaling-correction exponent ω related to the leading irrelevant operator: $\omega=1.0(1)$. Shorter Monte Carlo simulations of the bond-diluted bimodal models at $p_b=0.7$ and $p_b=0.35$ (up to $L=10$) and of the Ising spin glass model with Gaussian bond distribution (up to $L=8$) also support the existence of a unique Ising spin glass universality class. A careful finite-size analysis of the Monte Carlo data which takes into account the analytic and the nonanalytic corrections to scaling allows us to obtain precise and reliable estimates of the critical exponents. We obtain $\nu=2.45(15)$ and $\eta=-0.375(10)$.

DOI: 10.1103/PhysRevB.78.214205 PACS number(s): 75.10.Nr, 75.40.Mg, 75.40.Cx, 05.10.Ln

I. INTRODUCTION

The Ising model with random ferromagnetic (F) and antiferromagnetic couplings is a simplified model[1] for disordered uniaxial magnetic materials which show glassy (G) behavior in some region of their phase diagram such as $Fe_{1-x}Mn_xTiO_3$ and $Eu_{1-x}Ba_xMnO_3$ (see, e.g., Refs. 2–4). The random nature of the short-ranged interactions is mimicked by nearest-neighbor random bonds. This model is also interesting *per se* since it provides a laboratory in which the combined effects of quenched disorder and frustration can be studied.

It is now well established that three-dimensional Ising spin glass models present a high-temperature paramagnetic (P) phase and, for some values of the parameters, a low-temperature glassy phase (if the frustration is small, the low-temperature phase is ferromagnetic). The two phases are separated by a continuous phase transition, which is expected to belong to a unique universality class which is independent of the details of the model and, in particular, of the disorder distribution. Several numerical works[5–34] have addressed these issues, considering various Ising spin glass models, characterized by different disorder distributions, with or without dilution. Over the years many estimates of the critical exponents have been obtained. We mention the most recent ones for the correlation-length exponent ν: $\nu=2.39(5)$,[30] $\nu=2.72(8)$,[29] $\nu=1.5(3)$,[23] $\nu=1.35(10)$,[22] $\nu=2.15(15)$,[21] and $\nu=1.8(2)$,[20] obtained from simulations of the symmetric model with bimodal distribution; $\nu=2.22(15)$ for the bond-diluted symmetric bimodal model with $p_b=0.45$;[28] $\nu=2.44(9)$ (Ref. 30) and $\nu=2.00(15)$ (Ref. 18) for the symmetric model with Gaussian disorder distribution; and $\nu=2.4(6)$ for the random-anisotropy Heisenberg model in the limit of large anisotropy,[27] which is expected to be in the same Ising spin glass universality class.[27,35,36] Moreover, the analysis of different quantities has often given different estimates of the same critical exponent, even in the same model. For instance, recent Monte Carlo (MC) studies[29,30] find significant discrepancies among the estimates of the exponent ν obtained from the finite-size scaling (FSS) at T_c of the temperature derivative of ξ/L, of the Binder cumulant, and of the overlap susceptibility. For the bimodal Ising model Ref. 30 quotes $\nu=2.39(5)$, $\nu=2.79(11)$, and $\nu=1.527(8)$ from the analysis of these three quantities, respectively. A likely reason for these discrepancies is the presence of scaling corrections, which may be quite important in spin glass systems since the absence of fast MC algorithms makes it necessary to work with systems of relatively small size.

One of the aims of the present paper is a detailed analysis of the role of scaling corrections in spin glass systems. We present a general renormalization-group (RG) analysis based on the Wegner expansion,[37] which allows us to predict the corrections to the asymptotic critical behavior for the different quantities. In particular, we show that the analytic dependence of the relevant scaling fields on the model parameters, such as the temperature, may give rise to scaling corrections that decay as powers of $L^{-1/\nu}$, where L is the linear size of the lattice. Since $\nu\approx 2.45$ in Ising spin glass systems, they decay quite slowly and may give rise to systematic deviations, which are difficult to detect, given the small interval of values of L which can be considered in MC simulations. Their presence explains some inconsistencies in the standard analyses of MC data reported in the literature. Thus, it is crucial to take scaling corrections into account for an accurate study of the critical behavior, for a robust check of universality among different models, and for reliable estimates of universal quantities such as the critical exponents.

In this paper we report a high-statistics MC study of different Ising spin glass models. We consider the $\pm J$ Ising model for two values of the disorder parameter, the bond-diluted symmetric bimodal model with various values of the dilution, and also the model with Gaussian disorder distribution. We determine the FSS behavior of several RG invariant quantities such as the ratio $R_\xi \equiv \xi/L$ (ξ is the second-moment correlation length) and the quartic cumulants defined from the overlap variables. We verify with good precision their

independence on the model and disorder distribution, providing accurate evidence of universality. Then, we obtain an estimate of the leading correction-to-scaling exponent: $\omega = 1.0(1)$. Finally, we determine the critical exponents. We analyze the MC data at the critical point and in the high-temperature phase, taking into account the RG predictions for the scaling corrections and the precise above-reported estimate of ω. We obtain

$$\nu = 2.45(15),$$

$$\eta = -0.375(10). \quad (1)$$

Then, using scaling and hyperscaling relations we obtain

$$\beta = \nu(1+\eta)/2 = 0.77(5),$$

$$\gamma = (2-\eta)\nu = 5.8(4),$$

$$\alpha = 2 - 3\nu = -5.4(5). \quad (2)$$

In this work we extend the results presented in Ref. 32. First, we have significantly increased the statistics of the large-L data for the bimodal symmetric Ising model and we have added some data for other diluted models and for the symmetric model with Gaussian distributed couplings. Second, we present a much more detailed analysis of the critical-point data and an analysis of the high-temperature data obtained in the parallel-tempering simulations. This allows us to check the universality of the critical behavior of the correlation length and of the susceptibility in the high-temperature phase. Finally, we discuss the extended-scaling scheme,[29,38] which is inspired by the high-temperature expansion. As already noted in Ref. 29, this scheme shows an apparent improvement of the scaling behavior with respect to the naive approach in which scaling corrections are simply neglected, at least for some quantities, e.g., the overlap susceptibility. However, as we shall show, such an improvement is only marginal for the purpose of obtaining accurate results for the critical behavior at the transition. Indeed, this requires to take into account the analytic and nonanalytic scaling corrections predicted by the RG theory.

The paper is organized as follows. In Sec. II we define the models that we investigate and the quantities that are computed in the MC simulation. In Sec. III we derive the FSS predictions of the RG theory which are the basis of our FSS analyses. Details are reported in Appendix A. In Sec. IV and in Appendix B we give some details on the MC simulations. In Sec. V A we discuss universality, verifying that the infinite-volume limit of the quartic cumulants and of $R_\xi \equiv \xi/L$ is independent of the model. In Sec. V B we compute the leading correction-to-scaling exponent ω. In Sec. VI we compute the critical exponents ν and η and the critical temperature for the different models by using the data close to the critical point. In Sec. VII we present a global analysis of all available high-temperature data obtained in our parallel-tempering MC simulations. We again determine the critical exponents and show that the FSS behavior of several quantities is universal. Moreover, we discuss the extended-scaling scheme of Ref. 29. In Sec. VIII we compute the high-temperature zero-momentum quartic couplings. Finally, in Sec. IX we present our conclusions.

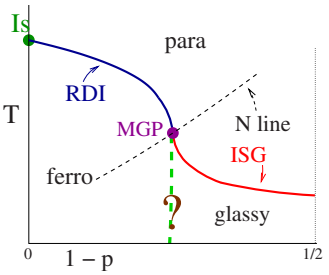

FIG. 1. (Color online) Phase diagram of the three-dimensional $\pm J$ (Edwards-Anderson) Ising model in the T-p plane for $p \geq 1/2$, i.e., $1-p \leq 1/2$. The phase diagram is symmetric under $p \to 1-p$.

II. ISING SPIN GLASS SYSTEMS

A. $\pm J$ Edwards-Anderson Ising model and its phase diagram

We consider the $\pm J$ Edwards-Anderson Ising model on a simple-cubic lattice of linear size L with periodic boundary conditions. The corresponding Hamiltonian is[1]

$$H = -\sum_{\langle xy \rangle} J_{xy}\sigma_x\sigma_y, \quad (3)$$

where $\sigma_x = \pm 1$, the sum is over the nearest-neighbor lattice sites, and the exchange interactions J_{xy} are uncorrelated quenched random variables with probability distribution

$$P(J_{xy}) = p\,\delta(J_{xy}-1) + (1-p)\,\delta(J_{xy}+1). \quad (4)$$

The usual bimodal Ising spin glass (ISG) model, for which $[J_{xy}]=0$ (square brackets indicate the average over the disorder distribution), corresponds to $p=1/2$. For $p \neq 1/2$ we have

$$[J_{xy}] = 2p - 1 \neq 0 \quad (5)$$

and ferromagnetic (or antiferromagnetic) configurations are energetically favored. Note that the free energy and also the correlations of the overlap variables that we shall define below are invariant under $p \to 1-p$ and thus we can always assume that $p \geq 1/2$.

The T-p phase diagram of the three-dimensional $\pm J$ Ising model is sketched in Fig. 1. The high-temperature phase is paramagnetic for any p. The nature of the low-temperature phase depends on the value of p. It is ferromagnetic for small values of $1-p$, while it is glassy with vanishing magnetization for sufficiently large values of $1-p$. The three phases are separated by transition lines, which meet at a magnetic-glassy multicritical point (MGP), usually called the Nishimori point, which is located along the so-called Nishimori line[39–43] defined by the relation $(p \geq 1/2)$

$$T = T_N(p), \quad T_N(p) = \frac{2}{\ln \dfrac{p}{1-p}}. \quad (6)$$

On the Nishimori line the magnetic and the overlap two-point correlation functions are equal.

The PF transition line starts at the Ising transition at $p=1$ and extends up to the MGP at $p=p^*$. For $p=1$ there is the standard Ising transition at[44] $T_{\rm Is}=4.511\ 524\ 8(6)$. Disorder is a relevant perturbation of the pure three-dimensional Ising fixed point. As a consequence, the Ising point $p=1$ is a multicritical point[45] with crossover exponent $\phi=\alpha_{\rm Is}$, where[46] $\alpha_{\rm Is}=0.109\ 6(5)$ is the Ising specific-heat exponent. The critical behavior for any $1>p>p^*$ belongs to the randomly dilute Ising (RDI) universality class[45] characterized by the correlation-length critical exponent[47,48] $\nu=0.683(2)$ and by the magnetic exponent $\eta=0.036(1)$. The coordinates of the MGP in the T-p plane are[43] $T^*=1.669\ 2(3)$ and $p^*=0.768\ 20(4)$. The multicritical behavior is characterized by[43] the thermal exponent $\nu=1.64(5)$, the crossover exponent $\phi=1.67(10)$, and the magnetic (and also overlap) exponent $\eta=-0.114(3)$.

The PG transition line starts at the MGP and extends up to $p=1/2$ [actually up to $p=1-p^*=0.231\ 80(4)$ due to the symmetry $p\to 1-p$ of the phase diagram]. A reasonable hypothesis is that the PG critical behavior is independent of p, as found in mean-field models.[49] Hence, for any $p^*>p>1-p^*$ the PG transition is expected to belong to the same universality class (named ISG in Fig. 1) as that of the bimodal Ising spin glass model at $p=1/2$. The critical behavior along this transition line is the main subject of this paper. As we shall see, the universality hypothesis is fully confirmed by our FSS analyses at $p=0.5$ and $p=0.7$.

The nature of the FG transition line is not clear yet. At fixed p the following inequality holds:[39,50]

$$|[\langle\sigma_x\sigma_y\rangle_T]| \le [|\langle\sigma_x\sigma_y\rangle_{T_N(p)}|], \tag{7}$$

where the subscripts indicate the temperature of the thermal average and $T_N(p)$ is the temperature along the Nishimori line, defined in Eq. (6). This relation shows that ferromagnetism can only exist in the region $p>p^*$ and that the system is maximally magnetized along the Nishimori line. Moreover, Ref. 51 (see also Refs. 42 and 52) argues that the FG transition line coincides with the line $p=p^*$ from $T=T^*$ to $T=0$. Recent numerical investigations[53–55] of the two-dimensional $\pm J$ model have shown that this conjecture is not exact, although quantitative deviations are small. At $T=0$ the critical value p_c where ferromagnetism disappears is definitely larger than p^*, indicating a reentrant transition line. In three dimensions Ref. 56 quotes $p_c=0.778(5)$, which is slightly larger than $p^*=0.768\ 20(4)$, with an associated critical exponent $\nu=1.1(3)$. It is therefore likely that the conjecture does not hold in three dimensions as well. We also mention that a mixed low-temperature phase,[57] in which ferromagnetism and (mean-field) glassy order coexist, is found in mean-field models[49] such as the infinite-range Sherrington-Kirkpatrick model.[58] Its presence has been confirmed in the $\pm J$ Ising model on a Bethe lattice.[59] However, there is no evidence of a mixed phase in the $\pm J$ Ising model on a cubic lattice[56] and in related models.[60] Nevertheless, the existence of such a mixed phase is still an open problem, as discussed in Ref. 59.

B. Other Ising spin glass models

We also consider the bond-diluted bimodal Ising model (BDBIM) defined by Hamiltonian (3) with bond probability distribution

$$P(J_{xy}) = p_b\left[\frac{1}{2}\delta(J_{xy}-J)+\frac{1}{2}\delta(J_{xy}+J)\right]+(1-p_b)\delta(J_{xy}). \tag{8}$$

A PG transition occurs for sufficiently small values of $1-p_b$, i.e., for $p_b>p_{\rm SG}$. While investigations at $T=0$ indicate that $p_{\rm SG}$ should be identified with the bond-percolation point[61,62] [$p_{\rm perc}=0.248\ 812\ 6(5)$ on a simple-cubic lattice[63]], recent investigations of the critical behavior close to the percolation point suggest that $p_{\rm SG}$ is larger than $p_{\rm perc}$.[64]

The model can be extended by considering the distribution

$$P(J_{xy}) = p_b[p\,\delta(J_{xy}-J)+(1-p)\,\delta(J_{xy}+J)]+(1-p_b)\delta(J_{xy}). \tag{9}$$

In this case, for $p_b>p_{\rm SG}$ ($p_{\rm SG}$ may depend on p) we expect a T-p phase diagram similar to the one sketched in Fig. 1 for the $\pm J$ Ising model without dilution, with a PF and a PG transition line meeting at a multicritical point.

A PG transition is also observed in the random-bond Ising spin glass model with Gaussian bond distribution

$$P(J_{xy}) = \frac{1}{\sqrt{2\pi}}e^{-J_{xy}^2/2}. \tag{10}$$

This transition is expected to be in the same universality class as that of the bimodal Ising model.[30]

C. Overlap thermodynamic quantities

In this work we focus on the critical behavior of the overlap parameter

$$q_x \equiv \sigma_x^{(1)}\sigma_x^{(2)}, \tag{11}$$

where the spins $\sigma_x^{(i)}$ belong to two independent replicas with the same disorder realization $\{J_{xy}\}$. The corresponding correlation function is

$$G(x) \equiv [\langle q_0 q_x\rangle] = [\langle\sigma_0\sigma_x\rangle^2], \tag{12}$$

where the angular and square brackets indicate the thermal average and the quenched average over $\{J_{xy}\}$, respectively. We define the susceptibility χ and the second-moment correlation length ξ as

$$\chi \equiv \sum_x G(x), \tag{13}$$

$$\xi^2 \equiv \frac{1}{4\sin^2(p_{\rm min}/2)}\frac{\tilde{G}(0)-\tilde{G}(p)}{\tilde{G}(p)}, \tag{14}$$

where $p=(p_{\rm min},0,0)$, $p_{\rm min}\equiv 2\pi/L$, and $\tilde{G}(q)$ is the Fourier transform of $G(x)$.

We also define the RG invariant quantities

$$R_\xi \equiv \xi/L, \tag{15}$$

$$U_4 \equiv \frac{[\mu_4]}{[\mu_2]^2}, \tag{16}$$

$$U_{22} \equiv \frac{[\mu_2^2]-[\mu_2]^2}{[\mu_2]^2}, \tag{17}$$

where

$$\mu_k \equiv \left\langle \left(\sum_x q_x \right)^k \right\rangle. \tag{18}$$

We call them phenomenological couplings and denote them by R in the following.

In the high-temperature paramagnetic phase, we also consider the zero-momentum quartic couplings

$$G_4 \equiv -\frac{\chi_4}{\xi^3 \chi^2}, \tag{19}$$

$$G_{22} \equiv -\frac{\chi_{22}}{\xi^3 \chi^2}, \tag{20}$$

where

$$\chi_4 \equiv \frac{1}{L^3}([\mu_4] - 3[\mu_2^2]), \tag{21}$$

$$\chi_{22} \equiv \frac{1}{L^3}([\mu_2^2] - [\mu_2]^2). \tag{22}$$

The critical limit $T \to T_c^+$ of the zero-momentum quartic couplings G_4 and G_{22} is universal.

III. FINITE-SIZE SCALING

In this section we summarize some basic results concerning FSS, which allow us to understand the role of the *analytic* and *nonanalytic* scaling corrections. We consider two Ising spin glass systems coupled by an interaction

$$h \sum_x q_x = h \sum_x \sigma_x^{(1)} \sigma_x^{(2)}, \tag{23}$$

where h is a constant external field. The model is defined on a cubic lattice of linear size L with periodic boundary conditions.

By applying standard RG arguments we expect the disorder-averaged free-energy density to be the sum of a regular part and a singular part,

$$\mathcal{F}(\beta,h,L) = \mathcal{F}_{\rm reg}(\beta,h,L) + \mathcal{F}_{\rm sing}(\beta,h,L), \tag{24}$$

where $\beta \equiv 1/T$. The regular part is expected to depend on L only through exponentially small terms, while the singular part encodes the critical behavior. The starting point of FSS is the scaling behavior of the singular part of the free-energy density (see, e.g., Refs. 37, 48, 65, and 66),

$$\mathcal{F}_{\rm sing}(\beta,h,L) = L^{-d} F(u_h L^{y_h}, u_t L^{y_t}, \{v_i L^{y_i}\}), \tag{25}$$

where d is the space dimension, u_h and u_t are the scaling fields associated with h and the reduced temperature $t \sim 1 - \beta/\beta_c$ [their RG dimensions are $y_h = (d+2-\eta)/2$ and $y_t = 1/\nu$, respectively], and v_i are irrelevant scaling fields with $y_i < 0$. At the critical point we have $u_t(t=0,h=0)=0$ and $u_h(t=0,h=0)=0$, while, generically, we expect $v_i(t=0,h=0) \neq 0$. Since $y_i<0$, for large L the free energy can be expanded in powers of $\{v_i L^{y_i}\}$. Therefore, we can write

$$\mathcal{F}_{\rm sing}(\beta,h,L) = L^{-d} f(u_h L^{y_h}, u_t L^{y_t}) + v_\omega L^{-d-\omega} f_\omega(u_h L^{y_h}, u_t L^{y_t}) + \cdots, \tag{26}$$

where the leading nonanalytic correction-to-scaling exponent ω is related to the RG dimension y_ω of the leading irrelevant scaling field $v_\omega \equiv v_1, \omega = -y_\omega$. The function $f(u_h L^{y_h}, u_t L^{y_t})$ is universal, once the scaling fields are properly normalized, for given boundary conditions and lattice geometry. The scaling fields are analytic functions of the system parameters—in particular, of h and t—and are expected not to depend on L. Note also that the size L is expected to be a nonlinear scaling field for periodic boundary conditions. For a general discussion of these issues, see Ref. 66, Sec. III of Ref. 67, and references therein. In general, u_t and u_h can be expanded as

$$u_h = h \bar{u}_h(t) + O(h^3), \quad \bar{u}_h(t) = a_h + a_1 t + O(t^2), \tag{27}$$

$$u_t = c_t t + c_{02} t^2 + c_{20} h^2 + c_{21} h^2 t + O(t^3, h^4, h^4 t), \tag{28}$$

where we used the fact that the free energy is symmetric under $h \to -h$. In the expansion of $u_{h,t}$ around the critical point $h,t=0$, the terms beyond the leading one give rise to analytic scaling corrections.

The scaling behavior of zero-momentum thermodynamic quantities can be obtained by performing appropriate derivatives of $\mathcal{F}$ with respect to h. For instance, for the overlap susceptibility at $h=0$ we obtain

$$\chi(\beta,L) = \left. \frac{\partial^2 \mathcal{F}}{\partial h^2} \right|_{h=0} = L^{2-\eta} \bar{u}_h(t)^2 g(u_t L^{y_t}) [1 + v_\omega L^{-\omega} g_\omega(u_t L^{y_t}) + \cdots] + g_{\rm reg}(\beta). \tag{29}$$

The function $g_{\rm reg}(\beta)$ represents the contribution of the regular part $\mathcal{F}_{\rm reg}(\beta,h,L)$ of the free-energy density and is L independent (apart from exponentially small terms). It gives rise to a correction proportional to $L^{\eta-2}$. Analogous formulas hold for the $2n$-point susceptibilities.

The FSS of the phenomenological couplings is given by

$$R(\beta,L) = r(u_t L^{y_t}) + v_\omega r_\omega(u_t L^{y_t}) L^{-\omega} + \cdots = R^* + r'(0) c_t t L^{y_t} + \cdots + c_\omega L^{-\omega} + \cdots, \tag{30}$$

where $R^* \equiv r(0)$, $c_\omega = v_\omega r_\omega(0)$, and the second line holds only very close to the critical point, for $t L^{y_t} \ll 1$. A proof of Eq. (30) for the phenomenological couplings U_4, U_{22}, and R_ξ is presented in Appendix A.

The thermal RG exponent $y_t=1/\nu$ is usually computed from the FSS of the derivative R' of a phenomenological coupling R with respect to β at β_c. Using Eq. (30) one obtains

$$R' \equiv \frac{\partial R}{\partial \beta} = L^{y_t}(\partial_\beta u_t)[r'(u_t L^{y_t}) + v_\omega L^{-\omega} r'_\omega(u_t L^{y_t}) + \cdots]. \tag{31}$$

One may also consider the derivative $\chi' \equiv d\chi/d\beta$ of the susceptibility χ. From Eq. (29) we obtain

$$\chi' = L^{2-\eta+y_t}\bar{u}_h^2 \partial_\beta u_t \{g'(u_t L^{y_t}) + v_\omega L^{-\omega}[g'(u_t L^{y_t}) g_\omega(u_t L^{y_t}) + g(u_t L^{y_t}) g'_\omega(u_t L^{y_t})]\} + 2L^{2-\eta}\bar{u}_h \partial_\beta \bar{u}_h g(u_t L^{y_t}) + \cdots + g'_{\rm reg}(\beta). \tag{32}$$

Note that the second term in the right-hand side gives rise to scaling corrections proportional to $L^{-y_t}=L^{-1/\nu}$, while the background term $g'_{\rm reg}(\beta)$ leads to corrections proportional to $L^{-y_t-2+\eta}$.

At $T=T_c$, setting $t=0$ in the above-reported equations, we obtain

$$R = R^* + c_\omega L^{-\omega} + \cdots, \tag{33}$$

$$\chi = cL^{2-\eta}(1 + c_\omega L^{-\omega} + \cdots), \tag{34}$$

$$R' = cL^{1/\nu}(1 + c_\omega L^{-\omega} + \cdots), \tag{35}$$

$$\chi' = cL^{2-\eta+1/\nu}(1 + c_\omega L^{-\omega} + \cdots + c_a L^{-1/\nu} + \cdots). \tag{36}$$

Note that, unlike the temperature derivative R' of a RG-invariant quantity, χ' also presents an $L^{-1/\nu}$ scaling correction due to the analytic dependence on t of the scaling field u_h (for this reason we call it analytic correction). Since, as we shall see, in the Ising spin glass case $1/\nu \approx 0.4$ and $\omega \approx 1.0$, the scaling corrections in χ' decay significantly more slowly than those occurring in R'. This makes the ratio

$$\frac{\chi'}{\chi} \sim L^{1/\nu} \tag{37}$$

unsuitable for a precise determination of ν and explains the significant discrepancies observed in Ref. 30.

Instead of computing the various quantities at fixed Hamiltonian parameters, one can also consider FSS keeping a phenomenological coupling R fixed at a given value R_f.[47,68] This means that, for each L, one determines $\beta_f(L,R_f)$ such that $R(\beta=\beta_f(L,R_f),L)=R_f$ and then considers any quantity at $\beta=\beta_f(L,R_f)$. The value R_f can be specified at will as long as R_f is taken between the high- and low-temperature fixed-point values of R. For $R_f \neq R^*$, where R^* is defined in Eq. (33), β_f converges to β_c as

$$\beta_f - \beta_c \sim L^{-1/\nu}, \tag{38}$$

while for $R_f=R^*$ we have

$$\beta_f - \beta_c \sim L^{-1/\nu-\omega}. \tag{39}$$

Indeed, if $u_{t,f}(L,R_f)$ is the value of u_t for $\beta=\beta_f(L,R_f)$, we obtain from Eq. (30)

$$u_{t,f} L^{y_t} = B(R_f) + v_\omega B_\omega(R_f) L^{-\omega} + \cdots, \tag{40}$$

where, using Eq. (30)),

$$r(B(x)) = x, \tag{41}$$

$$B_\omega(x) = -\frac{r_\omega(B(x))}{r'(B(x))}. \tag{42}$$

Now, if $R_f=R^*$, we have $B(R_f)=0$, which implies $u_{t,f} \sim L^{-y_t-\omega}$, hence Eq. (39). Otherwise, $B(R_f)$ is different from zero and we obtain behavior (38).

If we now substitute relation (40) into Eqs. (29)–(32), we obtain the expansion of the different quantities at fixed R_f, which we denote by adding a bar. Given $\mathcal{O}(\beta,L)$, we define $\bar{\mathcal{O}}(L,R_f) \equiv \mathcal{O}[\beta_f(L,R_f),L]$. For $R_f=R^*$, since $u_{t,f} \sim L^{-y_t-\omega}$ we reobtain Eqs. (33)–(36), with different coefficients, of course. If $R_f \neq R^*$, we must be more careful. The behavior of another phenomenological coupling R_α does not change qualitatively and we still have

$$\bar{R}_\alpha(L,R_f) \approx \bar{R}^*_\alpha + \bar{c}_\alpha L^{-\omega} + \cdots, \tag{43}$$

where $\bar{R}^*_\alpha = r_\alpha[B(R_f)]$ is universal. It depends on R_f and satisfies $\bar{R}^*_\alpha = R^*_\alpha$ for $R_f=R^*$. Also $\bar{\chi}'$ behaves as it does at fixed $T=T_c$; i.e., it follows Eq. (36). On the other hand, $\bar{\chi}$ and $\bar{R}'$ present additional analytic corrections. Indeed, since [see Eq. (27)]

$$\bar{u}_{h,f} = a_h + \frac{a_1}{c_t} B(R_f) L^{-y_t} + \cdots \tag{44}$$

[nonanalytic $O(L^{-\omega})$ corrections have been neglected], Eq. (29) gives

$$\bar{\chi}_\alpha(L,R_f) = L^{2-\eta}\left[a_h^2 + 2\frac{a_1 a_h}{c_t} B(R_f) L^{-y_t} + O(L^{-2y_t})\right] \times g(B(R_f))[1 + O(L^{-\omega})]. \tag{45}$$

If $R_f \neq R^*$, $B(R_f) \neq 0$, and thus analytic corrections occur. Note that, if R_f is close to R^*, since $B(R^*)=0$, we have

$$B(R_f) \sim R_f - R^*. \tag{46}$$

Hence, in this case the analytic corrections are small and of the order $(R_f-R^*)L^{-1/\nu}$. In general, corrections of the order $L^{-k/\nu}$ have amplitudes proportional to $(R_f-R^*)^k$.

IV. MONTE CARLO SIMULATIONS

In the MC simulations we employed the METROPOLIS algorithm, the random-exchange method (often called parallel-tempering or multiple Markov-chain method),[69] and multi-spin coding. See Appendix B for details on their implementation.

We simulated the $\pm J$ Ising model at $p=0.5$ for $L=3-14,16,20,24,28$ and $p=0.7$ for $L=3-12,14,16,20$ and the BDBIM at $p_b=0.45$ for $L=4-12,14,16$. We averaged over a large number N_s of disorder samples: $N_s \approx 6.4\times 10^6$ up to $L=12$, and $N_s/10^3 \approx 2400,2800,1500,245,150,18$, respectively, for $L=13,14,16,20,24,28$ in the case of the $\pm J$

TABLE I. Estimates of $\bar{U}_4$ at fixed $R_\xi=0.63$ for the $\pm J$ Ising model at $p=0.5$ and $p=0.7$ for the BDBIM at $p_b=0.45$, 0.7, and 0.35, and for the Ising spin glass model with Gaussian bond distribution.

L	$\pm J_{p=0.5}$	$\pm J_{p=0.7}$	BDBIM$_{p_b=0.45}$	BDBIM$_{p_b=0.7}$	BDBIM$_{p_b=0.35}$	Gaussian
4	1.48231(6)	1.46813(5)	1.49036(8)	1.48480(6)	1.49164(9)	1.49145(13)
5	1.48985(6)	1.47597(6)	1.49853(8)			1.4996(2)
6	1.49446(6)	1.48193(6)	1.50300(9)	1.49618(9)	1.50788(9)	1.5033(2)
7	1.49753(6)	1.48642(6)	1.50544(9)			
8	1.49987(6)	1.48984(6)	1.50714(9)	1.50082(9)	1.51320(13)	1.5063(5)
9	1.50136(6)	1.49260(6)	1.50815(9)			
10	1.50273(6)	1.49478(6)	1.50889(9)	1.50382(11)	1.5146(2)	
11	1.50383(6)	1.49665(6)	1.50946(9)			
12	1.50469(6)	1.49781(7)	1.50984(13)			
13	1.50541(11)					
14	1.50618(10)	1.50030(12)	1.5103(3)			
16	1.50702(13)	1.50220(13)	1.5113(3)			
20	1.5081(3)	1.5048(5)				
24	1.5089(4)					
28	1.5108(13)					

Ising model at $p=0.5$. Similar statistics were collected at $p=0.7$ (except for $L=20$ where the statistics were approximately 1/3 of those for $p=0.5$), while for the BDBIM statistics were smaller (typically, by a factor of 2 for the small lattices and by a factor of 6 for the largest ones). We also considered the BDBIM at $p_b=0.7$ and $p_b=0.35$ and the Ising model with Gaussian distributed couplings but only performed simulations for small values of L: $L=4,6,8,10$ for the BDBIM and $L=4,5,6,8$ for the Gaussian model.

For each L and model we performed parallel-tempering runs. This allowed us to estimate the different quantities in a large interval $[\beta_{\min},\beta_{\max}]$. To fix $\beta_{\max}$ we used the results of Ref. 30, which provided the best estimates of R_ξ^* at the time we started our simulations: 0.627(4) and 0.635(9) for an Ising model with bimodal and Gaussian distributed bonds, respectively. Thus, in most of the runs $\beta_{\max}$ was chosen, so that $R_\xi(\beta_{\max},L)\approx 0.63$. Only in the most recent simulations (two runs with $L=20$ and 24) of the $\pm J$ Ising model at $p=0.5$ did we take $\beta_{\max}$ such that $R_\xi(\beta_{\max},L)\approx 0.66$. We checked thermalization by using the recipe outlined in Ref. 30 (see Appendix B for details).

As already emphasized in Refs. 47 and 70, in high-precision MC studies of random systems one should be careful when computing disorder averages of products of thermal expectations, for instance, the cumulant U_{22} defined in Eq. (17). Indeed, naive estimators have a bias that may become significantly larger than the statistical error if N_s is large. We use (essentially) bias-free estimators defined as discussed in Ref. 47; some details are given in Appendix B.

In total, the MC simulations took approximately 40 years of CPU time on a single core of a 2.4 GHz AMD Opteron processor. The MC results which are used in the FSS analyses that follow can be found in Ref. 71.

V. UNIVERSALITY AND CORRECTION-TO-SCALING EXPONENT ω

A. Analysis of U_{22} and U_4 at fixed R_ξ

In this section we investigate the universality of the critical behavior of Ising spin glass models by comparing the limits for $L\to\infty$ of U_4 and U_{22} computed at fixed R_ξ, denoted by $\bar{U}_4$ and $\bar{U}_{22}$, respectively. As discussed in Sec. III, for sufficiently large L, $\bar{U}_4$ and $\bar{U}_{22}$ are expected to behave as

$$\bar{U}_\# = \bar{U}_\#^* + c_\# L^{-\omega}, \tag{47}$$

where the constants $\bar{U}_\#^*$ are universal (model independent) but depend on the fixed value of R_ξ; ω is the leading scaling-correction exponent.

In Tables I and II we report the estimates of $\bar{U}_4$ and $\bar{U}_{22}$ at fixed $R_\xi=0.63$ for different models. Without performing any analysis, one can immediately observe that the results obtained for the different models are very close and appear to approach the same large-L limit as L increases. For instance, the estimates of $\bar{U}_4$ for the largest lattices differ at most by 0.5%, while those of $\bar{U}_{22}$ vary by a few percent. This already provides a strong support to universality.

For a more detailed analysis, let us first consider the three models for which we have most data: the $\pm J$ model at $p=0.5$ and $p=0.7$ and the BDBIM at $p_b=0.45$. The MC estimates of $\bar{U}_4(L)$ are shown in Fig. 2 versus $1/L$. The results for the $\pm J$ Ising model at $p=0.5$ and $p=0.7$ fall quite nicely on two straight lines that approach the same point as $L\to\infty$. They support the universality of the critical behavior and show the presence of scaling corrections with an exponent $\omega\approx 1.0$. In the case of the BDBIM with $p_b=0.45$, the data apparently show a faster approach to the same infinite-

TABLE II. Estimates of $\bar{U}_{22}$ at fixed $R_\xi=0.63$ for the $\pm J$ Ising model at $p=0.5$ and $p=0.7$, for the BDBIM at $p_b=0.45$, 0.7, and 0.35, and for the Ising spin glass model with Gaussian bond distribution.

L	$\pm J_{p=0.5}$	$\pm J_{p=0.7}$	BDBIM$_{p_b=0.45}$	BDBIM$_{p_b=0.7}$	BDBIM$_{p_b=0.35}$	Gaussian
4	0.13714(6)	0.13955(6)	0.13581(9)	0.13602(7)	0.14635(10)	0.13522(15)
5	0.14088(7)	0.14087(6)	0.13935(10)			0.14014(24)
6	0.14277(7)	0.14181(7)	0.14166(10)	0.14193(10)	0.14501(10)	0.14227(24)
7	0.14392(6)	0.14262(7)	0.14308(10)			
8	0.14478(7)	0.14318(7)	0.14415(10)	0.14414(10)	0.14597(15)	0.1434(5)
9	0.14522(7)	0.14380(7)	0.14470(10)			
10	0.14561(7)	0.14418(7)	0.14518(10)	0.14536(12)	0.14586(24)	
11	0.14595(7)	0.14453(7)	0.14566(10)			
12	0.14618(7)	0.14465(7)	0.14605(14)			
13	0.14650(11)					
14	0.14671(10)	0.14531(13)	0.1462(3)			
16	0.14675(14)	0.14553(14)	0.1469(4)			
20	0.1469(4)	0.1458(5)				
24	0.1477(5)					
28	0.1496(14)					

volume limit. A fit of $\bar{U}_4(L)$ to $\bar{U}_4^*+cL^{-\varepsilon}$ using all data with $L>4$ gives an effective exponent $\varepsilon\approx 2$. However, for sufficiently large L, say $L\gtrsim 10$, scaling corrections are consistent with a linear $1/L$ behavior, as in the other models. The corresponding amplitude $|c_4|$ is quite small, at least a factor of 2 smaller than in the undiluted bimodal model. This means that for $L\lesssim 10$ next-to-leading corrections to scaling dominate and determine the apparent approach of the data to the infinite-volume limit. Since the ratios of the amplitudes of the leading scaling corrections are universal, a small $|c_4|$ implies that the leading nonanalytic scaling correction is small for any quantity. Thus, in this model the approach of any thermodynamic quantity to the critical limit should be faster than in the $\pm J$ models without dilution, as already noted in Ref. 28, at least for sufficiently large lattice sizes, where next-to-leading corrections can be neglected. Similar results are obtained for $\bar{U}_{22}$ (see Fig. 3). Only the points corresponding to $L=24,28$ and $p=0.5$ are slightly larger. In any case the differences are less than 1.5 error bars.

In order to estimate the universal infinite-volume values $\bar{U}_4^*$ and $\bar{U}_{22}^*$, we perform fits of $\bar{U}_\#$ to $\bar{U}_\#^*+c_\# L^{-\varepsilon}$. The exponent ε is either a free parameter or set equal to 1, which corresponds, as we discuss below, to our best estimate of the leading scaling-correction exponent ω. We repeat the fit several times, each time only including data such that $L\geq L_{\min}$. This allows us to check the dependence of the results on the neglected next-to-leading scaling corrections. In Table III we report the results. They are all consistent with the estimates

$$\bar{U}_4^*=1.514(2),\quad \bar{U}_{22}^*=0.148(1). \tag{48}$$

We can thus conclude that the estimates of $\bar{U}_4^*$ and $\bar{U}_{22}^*$ for the $\pm J$ Ising model and the BDBIM at $p_b=0.45$ are fully consistent with universality. The relative differences are ap-

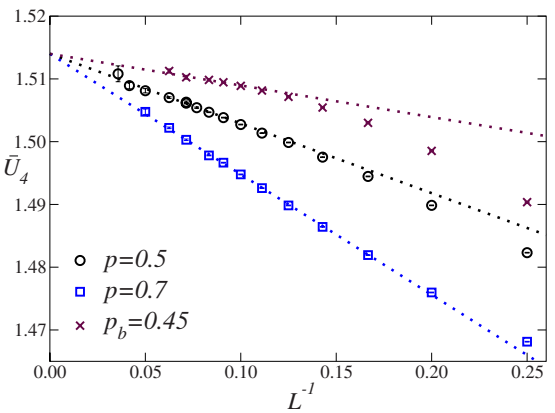

FIG. 2. (Color online) Estimates of $\bar{U}_4(L)$ vs L^{-1}, for the $\pm J$ model at $p=0.5$ and $p=0.7$ and the BDBIM at $p_b=0.45$. The dotted lines are drawn to guide the eyes.

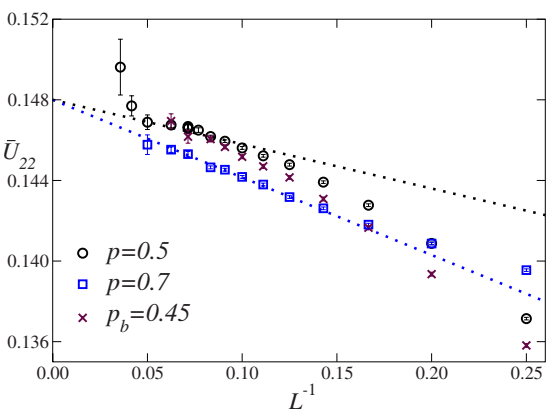

FIG. 3. (Color online) Estimates of $\bar{U}_{22}(L)$ vs L^{-1} for the $\pm J$ model at $p=0.5$ and $p=0.7$ and the BDBIM at $p_b=0.45$. The dotted lines are drawn to guide the eyes.

TABLE III. Results of the fits of $\bar{U}_4$ and $\bar{U}_{22}$ at fixed $R_\xi=0.63$ to $\bar{U}^*+cL^{-\varepsilon}$ for several values of $L_{\min}$, the minimum lattice size allowed in the fits. DOF is the number of degrees of freedom of the fit. The fits labeled "$p=0.5$ and $p=0.7$" are fits in which the data for $p=0.5$ and $p=0.7$ are analyzed together, assuming the universality of $\bar{U}_4^*$ and $\bar{U}_{22}^*$.

Model		$L_{\min}$	$\bar{U}_4^*$	χ^2/DOF	$\bar{U}_{22}^*$	χ^2/DOF
$\pm J, p=0.5$	Free ε	6	1.5127(4)	0.7	0.1478(3)	0.7
		8	1.5135(9)	0.8	0.1487(9)	0.7
		10	1.5119(11)	0.4	0.1482(12)	0.8
	$\varepsilon=1$	8	1.5144(2)	0.8	0.1490(2)	0.6
		12	1.5139(4)	0.6	0.1488(4)	0.9
$\pm J, p=0.7$	Free ε	6	1.5153(7)	2.0	0.1481(8)	0.8
		8	1.5145(14)	2.7	0.1471(9)	0.9
	$\varepsilon=1$	8	1.5143(2)	2.3	0.1478(2)	0.9
		12	1.5153(5)	0.1	0.1482(5)	0.8
BDBIM, $p_b=0.45$	Free ε	6	1.5120(3)	0.5	0.1479(6)	0.6
		9	1.5132(22)	0.6	0.1485(23)	0.5
	$\varepsilon=1$	8	1.5153(3)	0.8	0.1496(3)	0.4
		12	1.5148(12)	1.2	0.1489(13)	1.0
$\pm J, p=0.5$ and $p=0.7$	$\varepsilon=1$	8	1.5143(1)	1.2	0.1485(1)	2.1
		12	1.5145(3)	0.9	0.1486(3)	0.8
		16	1.5133(9)	0.4	0.1489(10)	1.1
	$\varepsilon=1.2$	8	1.5120(1)	4.9	0.1479(1)	2.5
		12	1.5127(3)	0.4	0.1482(3)	0.9
		16	1.5123(8)	0.3	0.1486(9)	1.1

proximately 1‰ in the case of $\bar{U}_4$ and 1% for $\bar{U}_{22}$.

We also considered the BDBIM for the other dilution values, i.e., for $p_b=0.7$ and $p_b=0.35$, though in this case we have data only up to $L=10$. The estimates of $\bar{U}_4$ are shown versus $1/L$ in Fig. 4. For $p_b=0.7$ scaling corrections clearly behave as $1/L$ and are larger than at $p_b=0.45$. For the scaling-correction amplitude c_4 defined in Eq. (47) we obtain the estimate $c_4\approx-0.10$ to be compared with the result c_4 ≈-0.11 for the $\pm J$ model at $p=0.5$ and $c_4\approx-0.05$ for the diluted model at $p_b=0.45$. For $p_b=0.35$ we do not have enough data to estimate c_4; however, the data reported in Fig. 4 apparently approach the infinite-volume limit faster than at $p_b=0.45$. As indicated by the MC data for $p_b\lesssim0.27$ of Ref. 64, the scaling corrections should increase as p_b further decreases. This suggests that the optimal model—the one with the smallest leading scaling corrections—corresponds to a dilution in the range $0.3\lesssim p_b^*\lesssim0.4$.

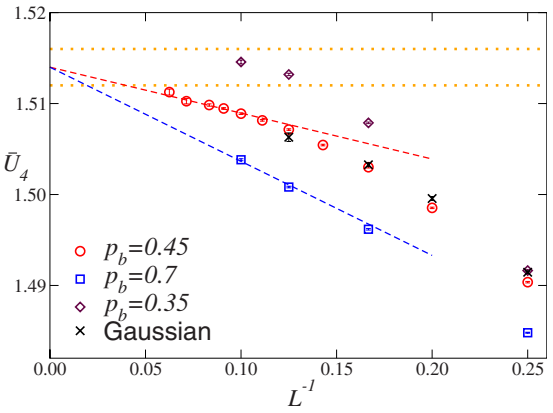

FIG. 4. (Color online) Estimates of $\bar{U}_4(L)$ for the BDBIM for several values of p_b and for the Ising spin glass model with Gaussian bond distribution. The dotted lines correspond to estimate (48), $\bar{U}_4^*=1.514(2)$. The dashed straight lines are extrapolations of the data at $p_b=0.7$ and $p_b=0.45$.

The estimates of $\bar{U}_4$ for the Ising spin glass model with Gaussian bond distribution are also shown in Fig. 4. They are very close and clearly approach estimate (48). The result for $L=8$ differs by 0.5% from the asymptotic value. Analogously, the data for $\bar{U}_{22}$ (see Table II) appear to approach asymptotic value (48). At $L=8$, $\bar{U}_{22}$ differs from $\bar{U}_{22}^*$ by 3%. In conclusion, the results for the $\pm J$ model, for the BDBIM, and for the model with Gaussian distributed couplings provide very strong evidence of universality for the critical behavior of Ising spin glass models along the PG transition line.

B. RG exponent of the leading irrelevant operator

The analyses of $\bar{U}_4$ and $\bar{U}_{22}$ also give estimates of ω. The most precise ones are obtained from fits of $\bar{U}_4$. Fits of $\bar{U}_4$ to $\bar{U}_4^*+c_pL^{-\omega}$ and of the difference $\bar{U}_4(p=0.5;L)-\bar{U}_4(p=0.7;L)$ to $bL^{-\omega}$ allow us to estimate

$$\omega = 1.0(1). \tag{49}$$

Consistent but less precise results are obtained from fits of $\bar{U}_{22}$. Result (49) is consistent with the less precise estimates $\omega = 0.84^{+0.43}_{-0.37}$ and $\omega = 1.0(4)$ reported in Refs. 21 and 27, respectively.

In order to verify that scaling corrections are controlled by a single correction-to-scaling term with exponent $\omega = 1$ and we have not determined an effective exponent arising from several almost degenerate exponents, we check that the ratio c_{22}/c_4 is universal, where $c_\#$ is the scaling-correction amplitude appearing in Eq. (47), as predicted by standard RG arguments. In order to determine this ratio, we fit together the available estimates of $\bar{U}(L)$ for the $\pm J$ Ising models at $p = 0.5$ and $p = 0.7$ to $\bar{U}(L) = \bar{U}^* + c_p L^{-\varepsilon}$, fixing $\varepsilon = 1$ and taking $\bar{U}^*$ and the two amplitudes $c_{p=0.5}$ and $c_{p=0.7}$ as free parameters. Fits of the data for $L \geq L_{\min} = 10$ give

$$\bar{U}^*_4 = 1.5142(2), \quad c_4(p = 0.5) = -0.114(2),$$

$$c_4(p = 0.7) = -0.194(2), \tag{50}$$

($\chi^2/\mathrm{DOF} \approx 1.3$, where DOF is the number of degrees of freedom of the fit), and

$$\bar{U}^*_{22} = 0.1484(2), \quad c_{22}(p = 0.5) = -0.027(2),$$

$$c_{22}(p = 0.7) = -0.044(2) \tag{51}$$

($\chi^2/\mathrm{DOF} \approx 1.4$). It follows that

$$c_{22}/c_4 = 0.24(2) \quad \text{for} \quad p = 0.5, \tag{52}$$

$$c_{22}/c_4 = 0.23(1) \quad \text{for} \quad p = 0.7, \tag{53}$$

which are in good agreement. These results are quite stable with increasing $L_{\min}$. For $L_{\min} = 12$ we obtain $c_{22}/c_4 = 0.24(3)$ and $c_{22}/c_4 = 0.24(2)$ for $p = 0.5$ and $p = 0.7$, while for $L_{\min} = 14$ we find $c_{22}/c_4 = 0.19(9)$ and $c_{22}/c_4 = 0.21(5)$, respectively; in both cases, the fits have $\chi^2/\mathrm{DOF} \lesssim 1$. Moreover, the variation in the ratio c_{22}/c_4 with respect to a change in the exponent ε by ± 0.1 (it corresponds to the uncertainty of ω) is smaller than the above-reported errors. These results fully support our interpretation of the $O(L^{-1.0})$ corrections as the corrections arising from the leading irrelevant scaling field.

VI. CRITICAL TEMPERATURE AND EXPONENTS

A. Estimates of β_c

In order to determine the critical temperature, we perform a standard FSS analysis of R_ξ, U_4, and U_{22}. Figure 5 shows the crossing points $\beta_{\mathrm{cross}}(L)$ determined by solving the equation

$$R(\beta_{\mathrm{cross}}, L) = R(\beta_{\mathrm{cross}}, 2L) \tag{54}$$

for the $\pm J$ Ising model at $p = 0.5$, using R_ξ and U_4. In the large-L limit $\beta_{\mathrm{cross}}(L)$ is expected to converge to β_c as

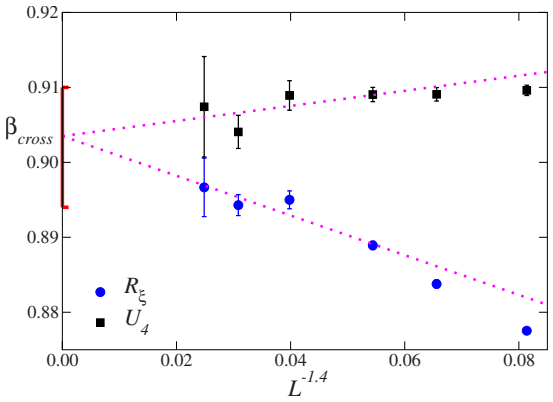

FIG. 5. (Color online) Crossing point $\beta_{\mathrm{cross}}(L)$ for the $\pm J$ Ising model at $p = 0.5$, from several pairs $L, 2L$, as obtained from R_ξ and U_4, versus $L^{-1/\nu-\omega} \sim L^{-1.4}$. The dotted lines show the result of a fit to $\beta_c + cL^{-1.4}$, which takes into account only the data satisfying $L \geq L_{\min} = 8$; it corresponds to $L^{-1.4}_{\min} \approx 0.054$. The bar along the y axis corresponds to the final estimate $\beta_c = 0.902(8)$.

$$\beta_{\mathrm{cross}}(L) - \beta_c \sim L^{-1/\nu-\omega} \sim L^{-1.4} \tag{55}$$

since $\nu \approx 2.45$ and $\omega \approx 1.0$. We perform a combined fit of β_{cross} for R_ξ and U_4 to $\beta_c + c_\# L^{-\varepsilon}$ with $\varepsilon = -1.4$, taking β_c and the two amplitudes c_{R_ξ} and c_{U_4} as free parameters. Using only the results with $L \geq L_{\min} = 8$, we obtain $\beta_c = 0.9035(22)$ with $\chi^2/\mathrm{DOF} \approx 1.1$ (since the estimates of R_ξ and U_4 are correlated, the error is only indicative). The corresponding lines are drawn in Fig. 5. We also consider larger values of $L_{\min}$. We find that the estimates of β_c vary significantly (much more than the statistical error) when $L_{\min}$ varies, indicating that the systematic error due to the additional scaling corrections is significantly larger than the statistical one. Equivalently, one can perform fits to

$$R(L, \beta_c) = R^* + bL^{-\omega}, \tag{56}$$

taking $R = R_\xi$ or U_4.[72] Taking into account the dependence of the results on $L_{\min}$ and their variation as ω varies by one error bar, we obtain the final estimates

$$\beta_c = 0.902(8), \quad T_c = 1.109(10). \tag{57}$$

We regard the error as conservative. We also consider the pseudocritical $\beta_f(L)$ defined in Sec. III at fixed R_ξ, which converges to β_c as $L \to \infty$ [cf. Eqs. (38) and (39)]. The results are consistent with estimate (57). The analysis of the crossing points and the fits to Eq. (56) also provide estimates of the limit $L \to \infty$ of R_ξ and U_4 at the critical point. We obtain

$$R^*_\xi = 0.645(15), \quad U^*_4 = 1.50(2). \tag{58}$$

Concerning the other models, similar analyses of R_ξ and U_4 give $\beta_c = 0.87(1)$ [$T_c = 1.149(13)$] for the $\pm J$ model at $p = 0.7$, and $\beta_c = 1.54(2)$ [$T_c = 0.649(8)$] for the BDBIM at $p_b = 0.45$. The corresponding values of R^*_ξ and U^*_4 are consistent with estimates (58). For comparison, we mention the result of Ref. 28 for the BDBIM at $p_b = 0.45$: $T_c = 0.663(6)$. Finally, in Fig. 6 we collect all results for the critical temperature T_c of the $\pm J$ Ising model at its various PF and PG transitions as a function of the disorder parameter p.

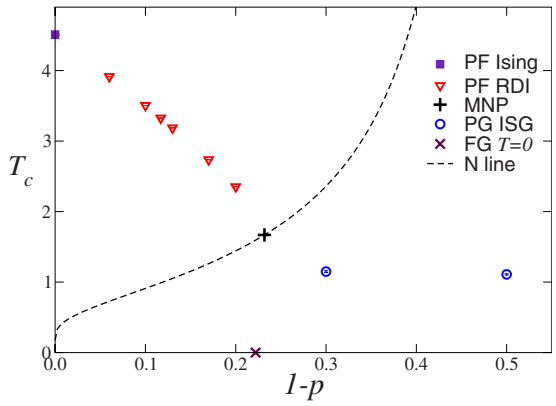

FIG. 6. (Color online) The values of the critical temperature T_c versus $1-p$ for the various transitions of the $\pm J$ Ising model. Besides the estimates for the PG ISG transitions, we also show results for the Ising transition at $p=1$, the PF RDI transitions, the location of the Nishimori point (MNP) along the N line, and the $T=0$ FG transition taken from Refs. 44, 45, 43, and 56, respectively.

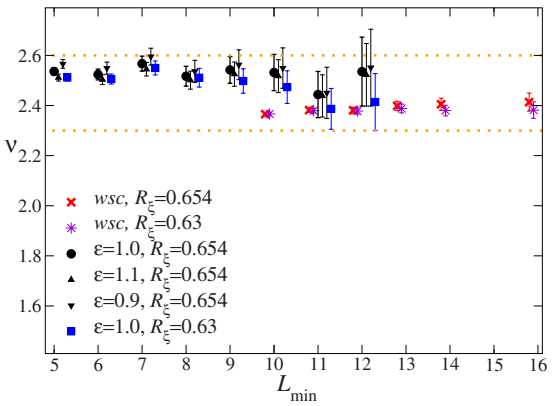

FIG. 7. (Color online) Estimates of the exponent ν from the analysis of $\bar{R}'_\xi$ at $R_\xi=0.63$ and $R_\xi=0.654$ for the $\pm J$ Ising model at $p=0.5$ obtained by fitting the data without scaling corrections (wsc) [Eq. (59)] and with scaling corrections [Eq. (60)]. We only show the results of the fits which satisfy $\chi^2/\mathrm{DOF}\lesssim 1.5$, up to values of $L_{\min}$ where the errors blow up. The dotted lines correspond to the final estimate $\nu=2.45(15)$.

B. Critical exponent ν

We estimate the critical exponent ν from the finite-size behavior of $R'_\xi \equiv dR_\xi/d\beta$ and $U'_4 \equiv dU_4/d\beta$ at a fixed value $R_{\xi,f}$ of R_ξ. As we discussed in Sec. III, the best choice for $R_{\xi,f}$ is R^*_ξ; otherwise, $\bar{R}'_\xi$ and $\bar{U}'_4$ present analytic corrections. In the present case, estimate (58) of R^*_ξ is not very precise; hence, the corrections of the order $L^{-1/\nu}\sim L^{-0.4}$ cannot be completely neglected. However, since their amplitude is proportional to $(R_\xi - R^*_\xi)$, we can assume that they are small for $R_{\xi,f}$ close to R^*_ξ. Thus, in order to estimate the systematic error induced by them, we proceed as follows. We perform the analysis of $\bar{R}'$ at fixed R_ξ using two different values of R_ξ and *neglecting* in both cases the $L^{-1/\nu}$ corrections. We use $R_\xi=0.630$ and $R_\xi=0.654$, which are close to our best estimate $R^*_\xi=0.645(15)$. For both values of R_ξ we determine an estimate of ν. Our final result is obtained by linear interpolation to $R_\xi=0.645$. The systematic error is estimated from the difference of the results at $R_\xi=0.630$ and $R_\xi=0.645$.

The exponent ν is obtained from fits of $\bar{R}'_\xi$ and $\bar{U}'_4$ to

$$\ln \bar{R}' = a + \frac{1}{\nu}\ln L, \tag{59}$$

$$\ln \bar{R}' = a + \frac{1}{\nu}\ln L + bL^{-\epsilon}, \tag{60}$$

with $\epsilon=\omega=1.0(1)$. The results of the fits of $\bar{R}'_\xi$ for the $\pm J$ Ising model with $p=0.5$ are shown in Fig. 7 as a function of the minimum lattice size $L_{\min}$ allowed in the fits. They are quite stable with respect to $L_{\min}$, depend very little on the fixed value R_ξ, and change only slightly as ω varies by ± 0.1, corresponding to one error bar. In particular, the fit of $\bar{R}'_\xi$ at $R_\xi=0.654$ to Eq. (60) gives $\nu=2.52(4)[2]$ ($\nu=2.53(7)[1]$) for $L\geq L_{\min}=8$ ($L_{\min}=10$); here the error in square brackets takes into account the uncertainty on ω. Analogously, the fit of the data at $R_\xi=0.630$ gives $\nu=2.51(4)[2]$ ($\nu=2.47(7)[1]$) for the same values of $L_{\min}$. In both cases $\chi^2/\mathrm{DOF}\approx 1.1$ ($\chi^2/\mathrm{DOF}\approx 1.3$). Therefore, we obtain $\nu=2.52(6)$ and 2.51(8) at $R_\xi=0.645$ for $L_{\min}=8,10$. The systematic error due to the analytic corrections is small, 0.01 and 0.04, for the two values of $L_{\min}$. The results from fits of $\bar{U}'_4$, which are shown in Fig. 8, favor a smaller value of ν, although in substantial agreement. Indeed, fits with $L_{\min}=10$ give $\nu=2.30(9)$ at $R_\xi=0.654$ and $\nu=2.42(9)$ at $R_\xi=0.630$, thus suggesting the estimate $\nu=2.35(9)$. The error due to the analytic corrections, which is approximately 0.07, is apparently larger than that obtained in the analysis of $\bar{R}'_\xi$, which is approximately 0.07. As our final result we take

$$\nu = 2.45(15), \tag{61}$$

which is consistent with the results obtained for $\bar{U}'_4$ and $\bar{R}'_\xi$.

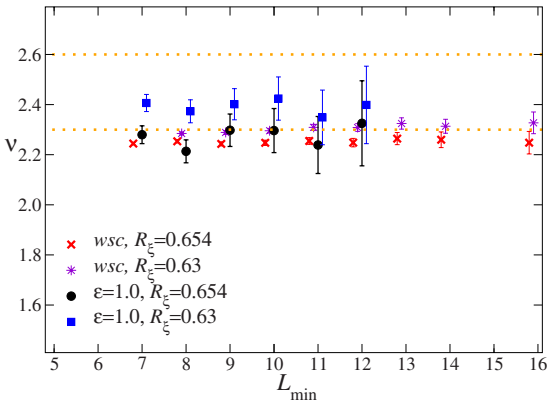

FIG. 8. (Color online) Estimates of the exponent ν from the analysis of $\bar{U}'_4$ at $R_\xi=0.63$ and $R_\xi=0.654$ for the $\pm J$ Ising model at $p=0.5$ obtained by fits without scaling corrections (wsc) [Eq. (59)] and fits with scaling corrections [Eq. (60)]. We only show the results of the fits which satisfy $\chi^2/\mathrm{DOF}\lesssim 1.5$, up to values of $L_{\min}$ where the errors blow up. The dotted lines correspond to $\nu=2.45(15)$.

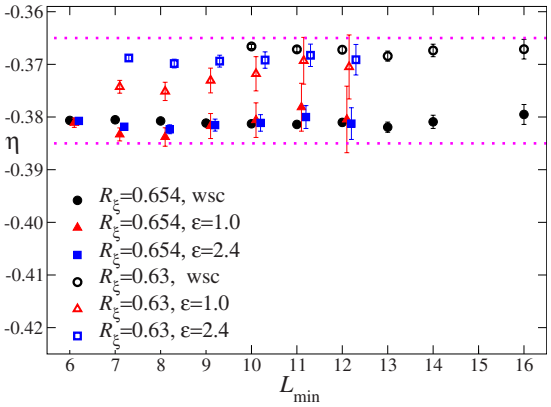

FIG. 9. (Color online) Estimates of the exponent η from the analysis of $\bar{\chi}(L,R_\xi)$ for $R_\xi=0.63$ and $R_\xi=0.654$ for the $\pm J$ Ising model at $p=0.5$. Only results of fits with $\chi^2/\mathrm{DOF}<1.5$ are shown. The dotted lines correspond to the estimate $\eta=-0.375(10)$.

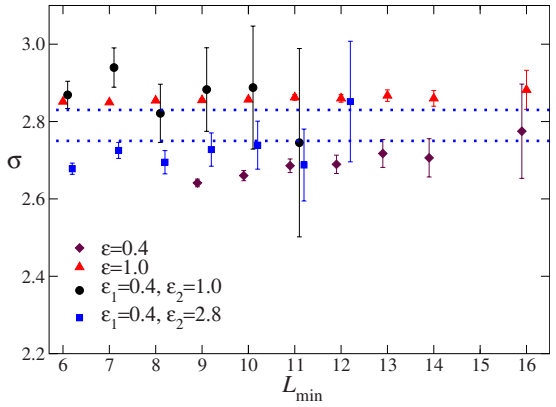

FIG. 10. (Color online) Estimates of the critical exponent $\sigma \equiv 1/\nu+2-\eta$, as obtained by analyzing $\bar{\chi}'$ at $R_\xi=0.654$. The dotted lines correspond to $\sigma=2.78(4)$.

Results at $R_\xi=0.63$ for the $\pm J$ model at $p=0.7$ and the BDBIM at $p_b=0.45$ are fully consistent with estimate (61). For the $\pm J$ model at $p=0.7$, fits with $\varepsilon=1.0$ and $L_{\min}=8$ of $\bar{R}'_\xi$ and $\bar{U}'_4$ at fixed $R_\xi=0.63$ give $\nu=2.49(5)$ and $\nu=2.37(6)$, respectively. In the case of the BDBIM at $p_b=0.45$ and again for $R_\xi=0.63$, fits without scaling corrections are in full agreement. Fits of $\bar{R}'_\xi$ to Eq. (60) assuming $\varepsilon=2.0$ are also consistent. For $L_{\min}=7$ they give $\nu=2.52(4)$. On the other hand, the fits of $\bar{U}'_4$ with $\varepsilon=2.0$ give results that are systematically larger; for instance, we obtain $\nu=2.61(5)$ for $L_{\min}=7$. This slight discrepancy is probably due to the fact that scaling corrections with exponent $\omega=1$ are small in the BDBIM at $p_b=0.45$ but not completely negligible; thus, the fits assume that corrections vanish faster than they really do, obtaining a slightly incorrect asymptotic estimate.

C. Critical exponent η

We estimate the exponent η by analyzing the susceptibility χ at fixed R_ξ. Its critical behavior is discussed in Sec. III. At fixed R_ξ, it behaves as

$$\bar{\chi}(L,R_\xi) = aL^{2-\eta}[1 + a_a(R_\xi - R_\xi^*)L^{-1/\nu} + \cdots + a_\omega L^{-\omega} + \cdots + a_b L^{-2+\eta} + \cdots], \tag{62}$$

where the $O(L^{-2+\eta})$ term is the background contribution [cf. Eq. (29)]. Since R_ξ is not exactly equal to R_ξ^*, we must take into account the $O(L^{-1/\nu})$ corrections. As for ν, the systematic error they induce is estimated by comparing the results at $R_\xi=0.630$ and $R_\xi=0.654$, which are close to the best estimate $R_\xi^*=0.645(15)$. We perform fits with and without scaling corrections, i.e., to

$$\ln \bar{\chi} = c + (2-\eta)\ln L, \tag{63}$$

$$\ln \bar{\chi} = c + (2-\eta)\ln L + c_\varepsilon L^{-\varepsilon}, \tag{64}$$

with $\varepsilon=1$ (the leading scaling correction arising from irrelevant scaling fields) and $\varepsilon=2.4\approx 2-\eta$ (to check the relevance of the background term, which might be large for small lattices) at $R_\xi=0.63$ and $R_\xi=0.654$. Figure 9 shows the estimates of η for the $\pm J$ model at $p=0.5$. As already mentioned, the systematic error due to the neglected $L^{-1/\nu}$ corrections is estimated from the difference of the estimates at $R_\xi=0.63$ and $R_\xi=0.654$. Following the same method used to determine ν, we obtain $\eta=-0.375(2)\{8\}$, where the first error is the statistical one, while the second error in curly braces takes into account the systematic error due to the residual $O(L^{-1/\nu})$ corrections and corresponds to the uncertainty on the estimate of R_ξ^*. Slightly smaller but perfectly consistent results are obtained in the analyses of the data for the other models. For example, in the case of the $\pm J$ Ising model at $p=0.7$, a fit of the data at $R_\xi=0.63$ to Eq. (64) with $\varepsilon=1.0$ gives $\eta=-0.381(5)$ for $L\geq L_{\min}=10$ ($\chi^2/\mathrm{DOF}\approx 1.6$). In the case of the BDBIM at $p_b=0.45$, a fit of the data at $R_\xi=0.63$ to Eq. (64) with $\varepsilon=2.0$ gives $\eta=-0.385(4)$ for $L\geq L_{\min}=9$ ($\chi^2/\mathrm{DOF}\approx 1.4$). Taking also these results into account, we arrive at the final estimate

$$\eta = -0.375(10). \tag{65}$$

We finally discuss the behavior of the derivative $\chi' \equiv d\chi/d\beta$ of the susceptibility, which in some numerical works (see, e.g., Ref. 30) has led to contradictory results for the exponent ν. We show in the following that this discrepancy is essentially due to the analytic $O(L^{-1/\nu})$ corrections discussed in Sec. III [cf. Eq. (36)]. At fixed R_ξ, $\bar{\chi}'$ is expected to behave as

$$\bar{\chi}'(L,R_\xi) = bL^\sigma[1 + b_a L^{-1/\nu} + \cdots + b_\omega L^{-\omega} + \cdots + b_b L^{-\sigma} + \cdots], \tag{66}$$

where $\sigma \equiv 1/\nu+2-\eta$. Using our best estimates of ν and η, we obtain $\sigma=2.78(4)$. Unlike the case of χ and the derivative of the phenomenological quantities, the amplitude b_a of the $O(L^{-1/\nu})$ corrections does not vanish at T_c and thus at $R_\xi=R_\xi^*$; therefore, it is not expected to be small when $R_\xi\approx R_\xi^*$. The $O(L^{-\sigma})$ term in Eq. (66) is the background contribution [cf. Eq. (32)]. In Fig. 10 we show the estimates of σ obtained in fits of $\ln \chi'$ to

$$\ln \bar{\chi}' = c + \sigma \ln L + c_\varepsilon L^{-\varepsilon},$$

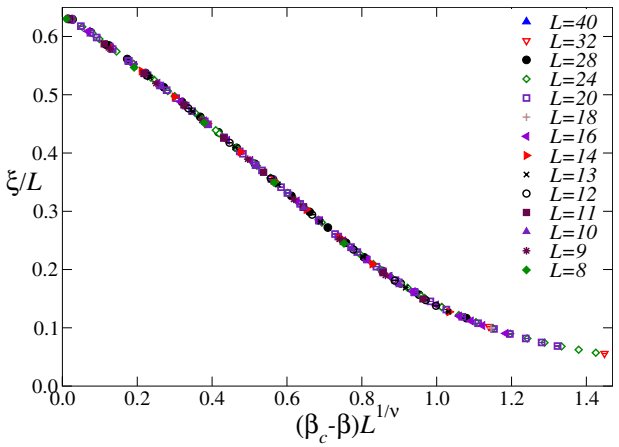

FIG. 11. (Color online) Plot of ξ/L vs $(\beta_c-\beta)L^{1/\nu}$ with $\beta_c=0.902$ and $\nu=2.45$. Data for the $\pm J$ model with $p=0.5$.

$$\ln \bar{\chi}' = c + \sigma \ln L + c_1 L^{-\varepsilon_1} + c_2 L^{-\varepsilon_2}, \tag{67}$$

for several values of $\varepsilon, \varepsilon_1, \varepsilon_2$. The results are consistent with the expected value $\sigma \approx 2.78$ when the $O(L^{-1/\nu})$ corrections are taken into account.

VII. HIGH-TEMPERATURE ESTIMATES

In the parallel-tempering simulations we have collected a large amount of data for several values of β in the high-temperature phase. They have not been used in the analyses we have presented in Secs. V and VI. Here, we shall present analyses that consider all high-temperature results. They fully confirm the critical-point estimates discussed above. We also show the universality of the finite-size scaling functions, providing additional evidence that all models belong to the same universality class.

A. Finite-size scaling behavior of ξ and estimates of ν

We determine ν from the FSS behavior of the correlation length. The starting point is the FSS equation

$$\frac{\xi(\beta,L)}{L} = f(u_t L^{1/\nu}) + \frac{v_\omega(\beta)}{L^\omega} f_\omega(u_t L^{1/\nu}) + \cdots, \tag{68}$$

where $f(x)$ and $f_\omega(x)$ are universal (once the normalization of the scaling fields has been fixed) and have a regular expansion in powers of x. In order to ensure a finite infinite-volume limit, for $x \to \infty$ they behave as

$$f(x) \sim x^{-\nu}, \quad f_\omega(x) \sim x^{\nu(\omega-1)}. \tag{69}$$

The scaling field u_t is an analytic function of β that vanishes at the critical point. Hence, it has an expansion

$$u_t = \beta_c - \beta + b(\beta_c-\beta)^2 + O[(\beta_c-\beta)^3]. \tag{70}$$

In Fig. 11 we report $\xi(\beta,L)/L$ versus $(\beta_c-\beta)L^{1/\nu}$ using the data for the $\pm J$ model at $p=0.5$ and the estimates of β_c and ν obtained in Sec. VI: $\beta_c=0.902$ and $\nu=2.45$. The data collapse quite precisely onto a single curve. This indicates that the nonanalytic scaling corrections are small and so are the analytic ones due to the nontrivial dependence of u_t on β.

In order to obtain quantitative estimates of ν, we follow Ref. 73 and perform three different fits of $\xi(\beta,L)/L$. In the first fit we neglect the nonanalytic scaling corrections, set $u_t=\beta_c-\beta$, and fit the data to (fit a)

$$\frac{\xi(\beta,L)}{L} = P_n(x)^{-\nu/n}, \quad x \equiv (\beta_c-\beta)L^{1/\nu}, \tag{71}$$

where $P_n(x)$ is a polynomial of degree n. We have chosen polynomials for computational convenience, but any other complete set of functions can be used. Note that specific choice (71) of fitting function satisfies large-x behavior (69). In this fit, the free parameters are the $(n+1)$ coefficients of the polynomial $P_n(x)$, the critical inverse temperature β_c, and ν.[74] The critical-point value R_ξ^* is equal to $P_n(x=0)^{-\nu/n}$.

In order to take into account the analytic corrections (fit b), we slightly modify *Ansatz* (71), setting $x \equiv \beta_c-\beta+b(\beta_c-\beta)^2$ and taking b as an additional free parameter. Finally, we consider the nonanalytic scaling corrections. We use the *Ansatz* (fit c)

$$\frac{\xi(\beta,L)}{L} = \left[P_n(x) + \frac{1}{L^\omega}(1+ax)^{\omega\nu} Q_n(x) \right]^{-\nu/n}, \quad x \equiv (\beta_c-\beta)L^{1/\nu}, \tag{72}$$

where $P_n(x)$ and $Q_n(x)$ are both polynomials of degree n and a is a free parameter. We can check that *Ansatz* (72) has the correct infinite-volume limit. For $L \to \infty$ at fixed β, i.e., for $x \to \infty$, we have $P_n(x) \approx p_n x^n$, $Q_n(x) \approx q_n x^n$, and

$$\begin{aligned} \xi(\beta,L) &\approx L\left[p_n x^n + \frac{1}{L^\omega}(ax)^{\omega\nu} q_n x^n \right]^{-\nu/n} \\ &\approx L x^{-\nu}[p_n + a^{\omega\nu} q_n (\beta_c-\beta)^{\omega\nu}]^{-\nu/n} \\ &\sim (\beta_c-\beta)^{-\nu}[1 + k(\beta_c-\beta)^\Delta], \end{aligned} \tag{73}$$

where $\Delta \equiv \omega\nu$. In these fits n must be chosen so that P_n provides an accurate parametrization of the scaling function. We have tried several values of n until the χ^2 of the fit does not change significantly as n increases by 1. In practice, we have taken n between 6 and 10. In fit (72) corrections to scaling are parametrized by a polynomial that has the same degree as that parametrizing the leading behavior. Our data are not so precise and corrections are not so large to require such a large number of parameters. To reduce the number of free parameters we have taken $n=6,9$ and set

$$Q_n(x) = q_0 + q_3 x^3 + \cdots + q_n x^n. \tag{74}$$

This *ad hoc* choice, which is arbitrary, significantly reduces the number of free parameters but still allows us to parametrize accurately (at the level of the statistical errors) the scaling corrections.

In order to take into account the additional scaling corrections which are not taken into account by our fit *Ansätze*, we have repeated each fit several times; each time we only include data such that $\beta \geq \beta_{\min}$ and $L \geq L_{\min}$. In Fig. 12 we report the estimates of ν obtained in fits of ξ/L to Eq. (71) for the $\pm J$ model at $p=0.5$. Corrections to scaling are clearly visible for small values of $\beta_{\min}$ and $L_{\min}$. Indeed, at fixed $L_{\min}$

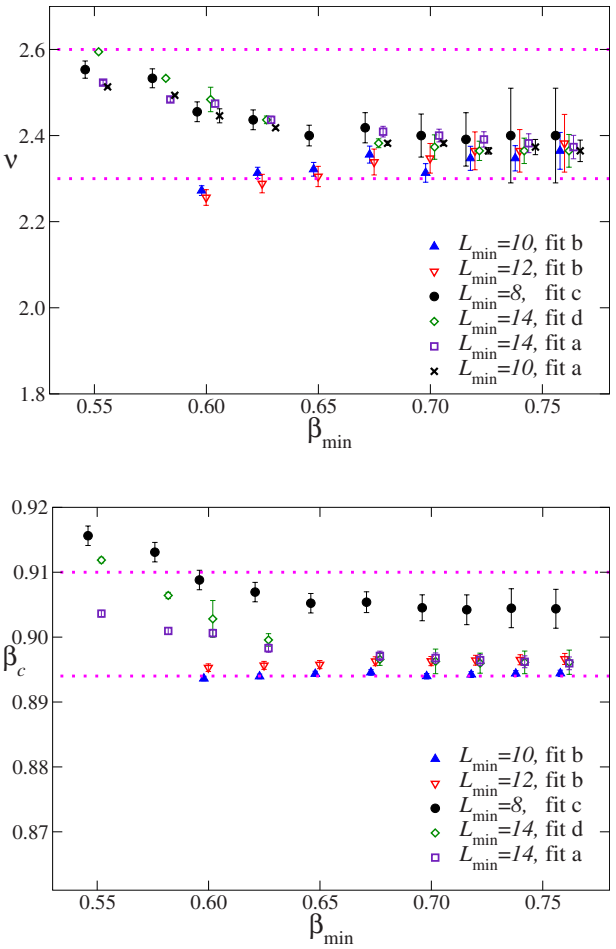

FIG. 12. (Color online) Estimates of ν (top) and β_c (bottom) for the $\pm J$ model at $p=0.5$. We report estimates obtained by fitting ξ/L to Eq. (71) (fit a), to Eq. (71) with $x \equiv [(\beta_c-\beta)+b(\beta_c-\beta)^2]L^{1/\nu}$ (fit b), to Eq. (72) with $\omega=1$ (fit c), and to extended-scaling *Ansatz* (86) (fit d). The dotted lines correspond to the estimates $\nu=2.45(15)$ (top) and $\beta_c=0.902(8)$ (bottom).

the estimates decrease, becoming approximately independent of $\beta_{\min}$ for $\beta_{\min} \gtrsim 0.65$. The dependence on $L_{\min}$ is instead tiny, and all results with $L_{\min} \geq 10$ are consistent within errors.

In Fig. 12 we also report the results of fits which take into account the analytic and the nonanalytic corrections (with $\omega=1$). As far as ν is concerned, no significant differences are observed and in all cases the results become independent of $\beta_{\min}$ for $\beta_{\min} \gtrsim 0.65$. All results (with their statistical errors) lie in the interval $2.3 \lesssim \nu \lesssim 2.5$, and are therefore in perfect agreement with the estimate $\nu=2.45(15)$ obtained before. Corrections to scaling are more evident in the analyses of β_c. Indeed, while analyses without nonanalytic scaling corrections give estimates of β_c that cluster around 0.895, those that take the corrections into account give values which are somewhat larger. In any case, all results are consistent with the estimate $\beta_c=0.902(8)$ obtained in Sec. VI A. Finally, these analyses also provide estimates of R_ξ^*. Analyses without nonanalytic scaling corrections give $R_\xi^*=0.632(5)$, while those which include scaling corrections give a somewhat higher value $R_\xi^*=0.648(5)$. Also in this case, scaling corrections appear to be quite relevant. These results are perfectly consistent with estimate (58), $R_\xi^*=0.645(15)$. The analyses that take into account the analytic scaling corrections (fit b) also give estimates of the constant b that appears in expansion (70) of u_t. They vary somewhat with $\beta_{\min}$ and give approximately $0 \lesssim b \lesssim 0.3$.

In order to verify universality, we compute ν and determine the FSS curves also for the $\pm J$ model at $p=0.7$ and the BDBIM at $p_b=0.45$. We report here only estimates of ν obtained by fitting the data to Eq. (71) since we do not have data precise enough to allow for a detailed study of the scaling corrections. In any case, the results for $p=0.5$ indicate that scaling corrections do not play much role in the determinations of ν. For the $\pm J$ model at $p=0.7$ we obtain $\nu=2.382(5)$ [$\nu=2.427(10)$] for $\beta_{\min}=0.59$ and $L_{\min}=7$ [$L_{\min}=9$] and $\nu=2.347(10)$ [$\nu=2.382(20)$] for $\beta_{\min}=0.68$ and the same values of $L_{\min}$. For the BDBIM at $p_b=0.45$ we obtain $\nu=2.574(6)$ [$\nu=2.637(7)$] for $\beta_{\min}=0.82$ and again $L_{\min}=7$ [$L_{\min}=9$] and $\nu=2.409(12)$ [$\nu=2.437(18)$] for $\beta_{\min}=1.02$. These results are in very good agreement with the estimate $\nu=2.45(15)$ reported above.

In order to verify the universality of the FSS curves we first fitted the data for the $\pm J$ model at $p=0.5$ presented in Fig. 11. Taking $\nu=2.45, \beta_c=0.902$ and using only the data satisfying $L \geq 10, \beta \geq 0.62$, we obtain

$$\frac{\xi}{L} = R_\xi(x), \quad x \equiv (\beta_c - \beta)L^{1/\nu} \tag{75}$$

with (this expression is valid in the interval of values of x for which we have data, i.e., for $0 \leq x \lesssim 1.5$)

$$\begin{aligned} R_\xi(x) = (&6.2828 + 16.8612x - 39.3317x^2 + 1926.5102x^3 \\ &- 17\,659.3388x^4 + 88\,711.1141x^5 - 256\,918.2481x^6 \\ &+ 446\,776.5137x^7 - 452\,723.8074x^8 \\ &+ 243\,001.4960x^9 - 50040.5243x^{10})^{-0.245}. \end{aligned} \tag{76}$$

The function $R_\xi(x)$ is universal apart from a rescaling of its argument. Thus, if we plot ξ/L vs $x \equiv (\beta_c-\beta)L^{1/\nu}$ in any model, the data should fall on the curve $R_\xi(cx)$, where c is a model-dependent constant. In Fig. 13 we report the data for the $\pm J$ model at $p=0.7$ and the BDBIM at $p_b=0.45$. The results show very good scaling and fall on top of the curve computed from the data of the bimodal model at $p=0.5$, confirming universality.

We finally consider the cumulant U_4. In the critical limit U_4 should be a universal function of ξ/L, independent of the model. Corrections scale as $L^{-\omega}h(\xi/L)$, where $h(x)$ is also universal, apart from a multiplicative constant. The numerical estimates of U_4 and ξ/L are reported in Fig. 14. We consider the $\pm J$ model at $p=0.5$ and $p=0.7$ and the BDBIM at $p_d=0.45$. We only consider the largest lattices, so that nonanalytic scaling corrections are not visible on the scale of the figure (a detailed study of the $L^{-\omega}$ corrections for $\xi/L=0.63$ is reported in Sec. V A). All points fall quite precisely onto a single curve, confirming that the PG transition in these three models belongs to the same universality class.

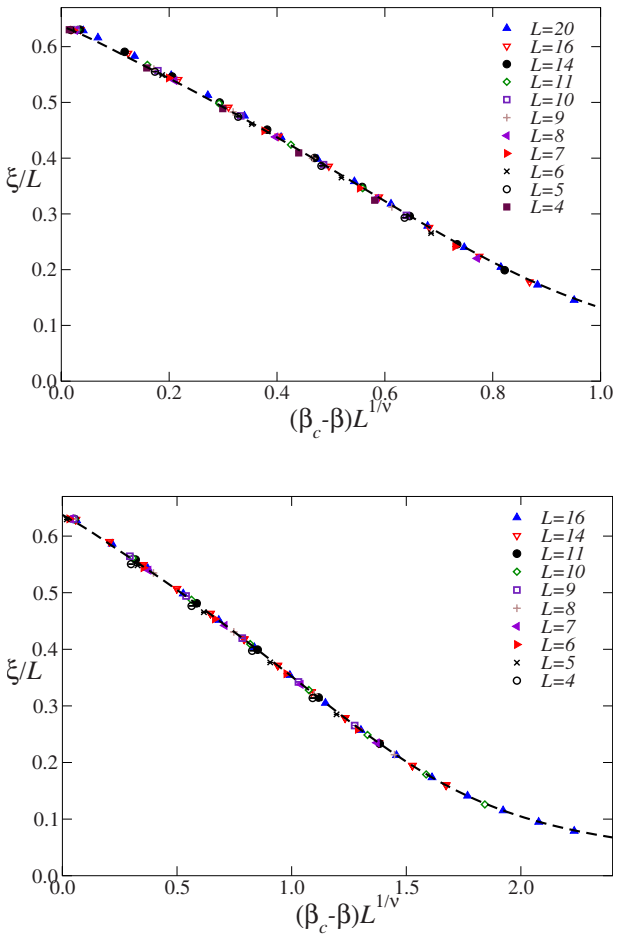

FIG. 13. (Color online) Plots of ξ/L vs $(\beta_c-\beta)L^{1/\nu}$ for the $\pm J$ model at $p=0.7$ (top) and for the BDBIM at $p_b=0.45$ (bottom). We use $\nu=2.45$, $\beta_c=0.87$ (top), and $\beta_c=1.54$ (bottom). The dashed line is the curve $R_\xi(cx)$, where $R_\xi(x)$ is function (76), which is estimated in fits of ξ/L for the $\pm J$ model at $p=0.5$, and c is a model-dependent constant: $c\approx 1.026$ for the $\pm J$ model at $p=0.7$ and $c\approx 0.5641$ for the BDBIM at $p_b=0.45$.

B. Finite-size scaling of the susceptibility and estimates of η

We now turn to the determination of the critical exponent η. The starting point is Eq. (29), which we rewrite as

$$\chi(\beta,L) = L^{2-\eta}\bar{u}_h(\beta)^2 g(u_t L^{1/\nu})\left[1+\frac{v_\omega(\beta)}{L^\omega} g_\omega(u_t L^{1/\nu})+\cdots\right]. \tag{77}$$

This equation is not very convenient since it involves u_t, and hence the critical temperature and the exponent ν. To reduce the number of unknown parameters, we note that Eq. (68) can be inverted to give

$$u_t L^{1/\nu} = F(\xi/L) + \frac{v_\omega(\beta)}{L^\omega} F_\omega(\xi/L) + \cdots. \tag{78}$$

Inserting this expression in Eq. (77) we obtain the scaling form

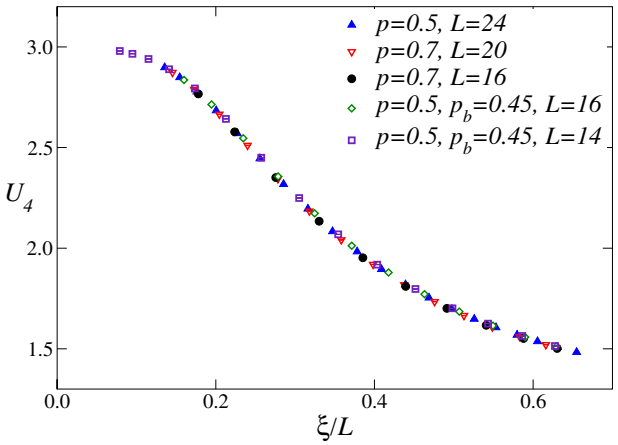

FIG. 14. (Color online) Plot of U_4 vs ξ/L for the $\pm J$ model at $p=0.5$ and 0.7 and the BDBIM at $p_b=0.45$.

$$\chi(\beta,L) = \xi^{2-\eta}\bar{u}_h(\beta)^2 C(\xi/L)[1+v_\omega(\beta)\xi^{-\omega}C_\omega(\xi/L)+\cdots]. \tag{79}$$

In Eq. (79) we have singled out $\xi^{2-\eta}$ and $\xi^{-\omega}$ instead of $L^{2-\eta}$ and $L^{-\omega}$. With this choice $C(x)$ and $C_\omega(x)$ are regular for $x\to 0$. Note the presence of the function $\bar{u}_h(\beta)$. In the FSS limit $\xi\to\infty$, $L\to\infty$ at fixed ξ/L, we have $\beta\to\beta_c$, so that asymptotically it should be possible to replace $\bar{u}_h(\beta)$ with the constant $\bar{u}_h(\beta_c)$. Therefore, this function gives rise to scaling corrections that we have named analytic corrections in Sec. III. In order to understand their relevance for our data, in Fig. 15 (upper panel) we plot $\xi^{\eta-2}\chi$ versus ξ/L for the $\pm J$ model at $p=0.5$. It is evident that the data do not fall onto a single curve. The scaling-field term $\bar{u}_h(\beta)$ varies significantly with β and therefore cannot be neglected.

The previous discussion indicates that, in order to estimate accurately the exponent η, it is essential to include the analytic corrections in the fitting function. We perform two fits. In the first one (fit a) we neglect the nonanalytic scaling corrections and consider

$$\ln\frac{\chi}{\xi^2} = -\eta\ln\xi + P_n(\xi/L) + Q_m(\beta), \tag{80}$$

where $P_n(x)$ and $Q_m(x)$ are polynomials of degree n and m, respectively. Moreover, we require $Q_m(0)=0$ in order to avoid the presence of two constant terms. As before, n and m are varied until the quality of the fit does not change significantly by varying the parameters by 1. In practice, we take $6\le n,m\le 10$. To include the scaling corrections, we also consider

$$\ln\frac{\chi}{\xi^2} = -\eta\ln\xi + P_n(\xi/L) + Q_m(\beta) + \xi^{-\omega}S_p(\xi/L), \tag{81}$$

where $S_p(x)$ is a polynomial of degree p. We take $p\le 3$. Note that here, as we already did in the analysis of ξ/L, we neglect the β dependence of the scaling field v_ω.

The results of the fits for the $\pm J$ model at $p=0.5$ are reported in Fig. 16. The estimates of the fit to Eq. (80) are very stable and show a very tiny dependence on $\beta_{\min}$ and $L_{\min}$. For instance, for $\beta_{\min}=0.55$ we obtain $\eta=-0.3636(8)$

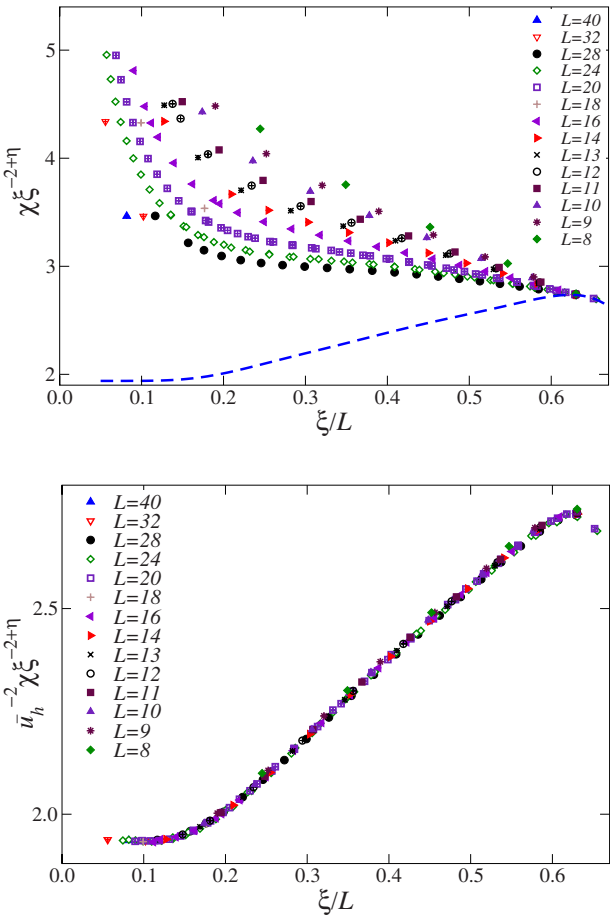

FIG. 15. (Color online) Plots of $\chi\xi^{\eta-2}$ (upper panel) and of $\chi\xi^{\eta-2}\tilde{u}_h^{-2}$ (lower panel) vs ξ/L with $\eta=-0.375$. The dashed line in the upper panel is the universal curve $\tilde{C}(\xi/L)$, as estimated in fits of χ to Eq. (80). Data for the $\pm J$ model at $p=0.5$.

$(L_{\min}=8)$ and $\eta=-0.3659(27)$ $(L_{\min}=14)$, while for $\beta_{\min}=0.75$ we have $\eta=-0.3666(10)$ $(L_{\min}=8)$ and $\eta=-0.3657(31)$ $(L_{\min}=14)$. Fits with nonanalytic scaling corrections are less stable. We observe significant fluctuations that indicate that the data are not precise enough to be sensitive to this type of scaling corrections. This is consistent with what is observed at the critical point. While the results for η depend strongly on the chosen value for $R_{\xi,f}$, indicating that the analytic scaling corrections are important, essentially no dependence is observed on the nonanalytic ones (see, e.g., Fig. 9). In any case, all results are consistent with the estimate $\eta=-0.375(10)$ obtained in Sec. VI C.

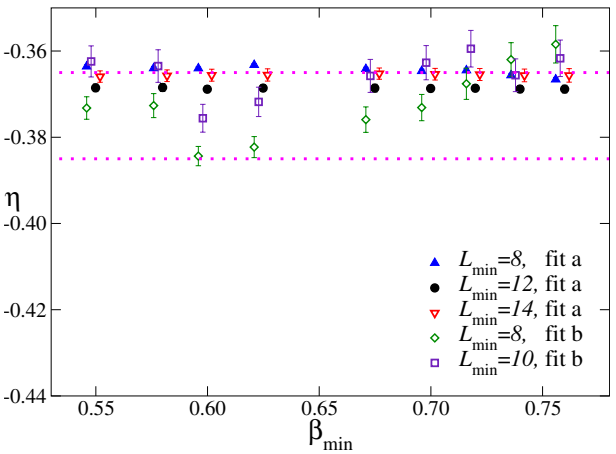

FIG. 16. (Color online) Estimates of η for the $\pm J$ model at $p=0.5$. We report estimates obtained by fitting χ to *Ansatz* (80) (fit a) and *Ansatz* (81) (fit b) for several values of $L_{\min}$ and $\beta_{\min}$. The dotted lines correspond to the estimate $\eta=-0.375(10)$.

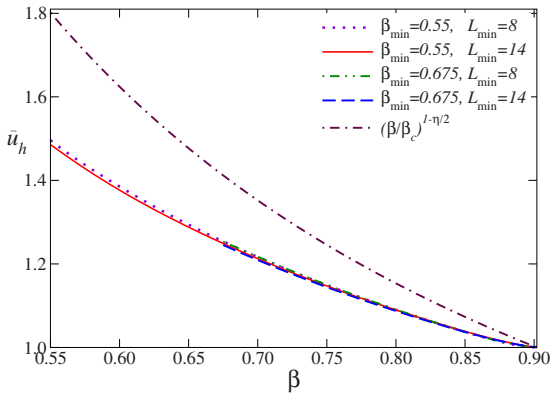

FIG. 17. (Color online) Scaling-field function $\tilde{u}_h(\beta)$ for the $\pm J$ model at $p=0.5$, as determined in the fits of χ to *Ansatz* (80), for different values of $\beta_{\min}$ and $L_{\min}$. It is normalized such that $\tilde{u}_h(\beta_c)=1$. We also report the approximation $\tilde{u}_h(\beta)\approx(\beta/\beta_c)^{1-\eta/2}$, which is used in the extended-scaling scheme (see the discussion in Sec. VII C).

The fits also give estimates of the function $\bar{u}_h(\beta)$ that appears in Eqs. (77) and (79). In Fig. 17 we plot $\tilde{u}_h(\beta)=\bar{u}_h(\beta)/\bar{u}_h(\beta_c)$ [$\tilde{u}_h(\beta)$ is normalized, so that $\tilde{u}_h(\beta_c)=1$] as obtained in the different fits. The results corresponding to different values of $L_{\min}$ and $\beta_{\min}$ agree nicely, supporting scaling *Ansatz* (79). A simple expression which reproduces the results reported in Fig. 17 is

$$\tilde{u}_h(\beta) = 1 + 0.556\,247(1-\beta/0.902) + 1.833\,22(1-\beta/0.902)^2, \quad (82)$$

which is valid for $0.55\leq\beta\leq0.902$. Once $\tilde{u}_h(\beta)$ has been determined, we can compute the scaling function $\tilde{C}(\xi/L)=\bar{u}_h(\beta_c)^2C(\xi/L)$ by considering $L^{\eta-2}\chi\tilde{u}_h(\beta)^{-2}$. Such a combination is shown in Fig. 15 (lower panel). All points fall on top of each other, confirming the validity of the FSS *Ansatz*. Moreover, as expected, we find that $\tilde{C}(0)$ is finite and $\tilde{C}(\xi/L)$ is approximately constant for $\xi/L\lesssim0.15$, two properties which are not obvious from the upper panel of Fig. 15. These conclusions are consistent with the FSS results for $\chi(2L,\beta)/\chi(L,\beta)$ [in this quantity the analytic function $\bar{u}_h(\beta)$ cancels out] reported in Refs. 20 and 28, which show that this ratio has a tiny dependence on ξ/L up to $\xi/L\approx0.15$ [for $\xi/L=0.15$ we have $\chi(2L,\beta)/\chi(L,\beta)\approx1.02$]. Note that the curve in the lower panel of Fig. 15 (which corresponds to the dashed line in the upper panel) is the limiting curve of the points that appear in the upper panel as $L\to\infty$. Since the rate of convergence is very slow (at fixed ξ/L data converge as $L^{-1/\nu}$), it is clear that such an asymptotic behavior can only

be observed on enormously large lattices. Thus, in order to estimate η, it is crucial to take the function $\bar{u}_h(\beta)$ into account.

The function $\widetilde{C}(x)$ is universal, apart from a model-dependent multiplicative constant. We write it as

$$\widetilde{C}(x) = b\Gamma(x), \quad \Gamma(0) = 1, \tag{83}$$

where $\Gamma(x)$ is universal. A fit of the data reported in Fig. 15 gives

$$\Gamma(x) = 1 + 5.9622y - 104.4625y^2 + 1516.2443y^3 - 12\,260.6638y^4 + 50\,105.6104y^5 - 80\,471.2150y^6,$$

$$y \equiv \exp(-1/x), \tag{84}$$

and $b \approx 1.9395$. Expression (84) is valid for $x \equiv \xi/L \lesssim R_\xi^* \approx 0.645$.

The same analyses can be repeated for the $\pm J$ model at $p=0.7$ and the BDBIM at $p_b=0.45$. Here we only present results corresponding to fits to *Ansatz* (80). Our data are not precise enough to allow us to perform fits which include the nonanalytic scaling corrections. The results are consistent with the estimate $\eta=-0.375(10)$. For the $\pm J$ model at $p=0.7$, we obtain $\eta=-0.366(2)$ ($\beta_{\min}=0.59$) and $\eta=-0.366(3)$ ($\beta_{\min}=0.68$) for $L_{\min}=7$ and $\eta=-0.368(2)$ ($\beta_{\min}=0.59$) and $\eta=-0.366(3)$ ($\beta_{\min}=0.68$) for $L_{\min}=9$. For the BDBIM, we obtain $\eta=-0.361(2)$ and $-0.359(3)$ for $L_{\min}=7$ and 9 and any $\beta_{\min}$ in the range [0.82,1.12].

As a further check of universality we determine the scaling behavior of the combination $\chi\xi^{\eta-2}\widetilde{u}_h^{-2}$. In Fig. 18 we report this quantity for the $\pm J$ model at $p=0.7$ (upper panel) and the BDBIM at $p_b=0.45$ (lower panel), using in both cases $\eta=-0.375$ and our best estimate of $\widetilde{u}_h$. As expected all points fall onto a single curve. If universality holds, these curves should be parametrized as $b\Gamma(x)$, where $\Gamma(x)$ is given in Eq. (84) and b is a model-dependent constant. In the case of the $\pm J$ model (upper panel of Fig. 18) we observe very good agreement, while for the BDBIM at $p_b=0.45$ (lower panel) some discrepancies occur for $\xi/L \gtrsim 0.4$. There are two reasons for them. First, the function $\widetilde{u}_h$ is not precisely known for $\beta \approx \beta_c$. In this range of values of β it varies slightly (10%) with $\beta_{\min}$ and $L_{\min}$. Second, the plot depends on η. If we increase η by one error bar, discrepancies are significantly reduced.

It is worth noting that the functions $\bar{u}_h$ are approximately the same in the three models we study, if one considers them as a function of the reduced temperature $t \equiv 1-\beta/\beta_c$. For $0 \lesssim t \lesssim 0.4$—this is the interval of t which is probed by our simulations—the ratio $\bar{u}_{h,\text{model }1}(t)/\bar{u}_{h,\text{model }2}(t)$ is constant, within our precision, for any pair of models. This result is somewhat unexpected within RG theory because these functions are not universal.

Finally, let us comment on the FSS approach of Ref. 75 applied to spin glass systems in Refs. 20 and 28. In this approach one considers the ratio $\chi(2L,\beta)/\chi(L,\beta)$. This choice has a significant advantage. The scaling-field function $\bar{u}_h(\beta)$ cancels out, so that the leading scaling corrections are the nonanalytic ones. As we have shown here, they are quite small, so that very good scaling is observed and reliable

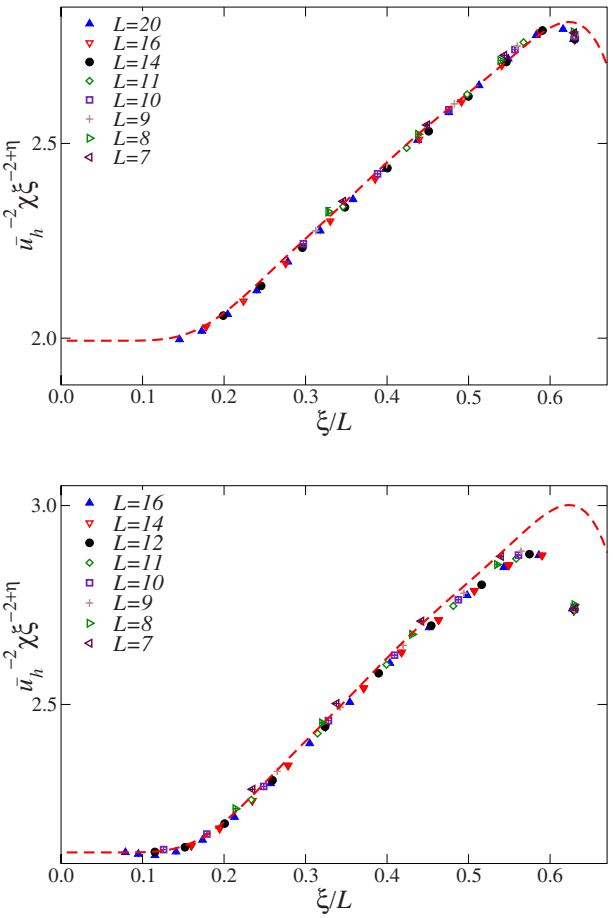

FIG. 18. (Color online) Plot of $\chi\xi^{\eta-2}\widetilde{u}_h^{-2}$ vs ξ/L for the $\pm J$ model at $p=0.7$ with $\eta=-0.375$ (upper panel) and for the BDBIM at $p_b=0.45$ with $\eta=-0.375$ (lower panel). In each panel we report the curve $b\Gamma(\xi/L)$, where $\Gamma(\xi/L)$ is defined in Eq. (84) and b is a model-dependent constant. We use $b=1.993\,46$ and $2.127\,94$ in the upper and lower panels, respectively. They are determined by requiring a perfect fit for $\xi/L \lesssim 0.2$.

infinite-volume estimates are obtained. Analytic scaling corrections come in again when considering the critical limit of the infinite-volume results $\chi_\infty(\beta)$. Indeed, since $\Delta \equiv \omega\nu \approx 2.45$, for $\beta \to \beta_c$ the analytic corrections dominate,

$$\chi_\infty(\beta) = (\beta_c-\beta)^{-\gamma}[b_0 + b_1(\beta_c-\beta) + b_2(\beta_c-\beta)^2 + b_\Delta(\beta_c-\beta)^\Delta + \cdots]. \tag{85}$$

C. Extended-scaling scheme

In this section we consider the extended-scaling scheme introduced in Ref. 29. It consists of a particular choice of scaling variables, which, according to Ref. 29, should somehow decrease scaling corrections and thus allow a faster convergence to the critical limit. Let us consider first ξ/L. In this scheme the appropriate fit *Ansatz* is

$$\frac{\xi(\beta,L)}{L} = P_n(x)^{-\nu/n}, \quad x \equiv (\beta_c^2-\beta^2)(L/\beta)^{1/\nu}, \tag{86}$$

where $P_n(x)$ is a polynomial of degree n. The results for the $\pm J$ model at $p=0.5$ are reported in Fig. 12 and should be

compared with those obtained by fits to Eq. (71), which neglect any scaling corrections (fit a). They are substantially equivalent. This can be explained by noting that, for the present values of β_c and ν, we have

$$(\beta_c^2 - \beta^2)\beta^{-1/\nu} = 1.88(\beta_c - \beta)[1 - 0.10(\beta_c - \beta) + \cdots]. \tag{87}$$

Thus, fit (86) is essentially equivalent to a fit with analytic corrections (fit b) with $b=-0.10$. Such a value of b is small—hence, this change in the scaling variable does not have much influence on the final results—and is close to what we obtain numerically, although not fully consistent (we predict $0 \lesssim b \lesssim 0.3$). We also tried fits with $x \equiv (\beta_c^2 - \beta^2)L^{1/\nu}$, which might be thought as a natural variable in spin glass systems, given the symmetry under $\beta \to -\beta$.[24] These fits are significantly worse than the previous ones for $\beta_{\min} \lesssim 0.70$. For larger values, no significant differences are observed. These results can be understood by noting $(\beta_c^2 - \beta^2) = 1.80(\beta_c - \beta)[1 - 0.55(\beta_c - \beta) + \cdots]$. Thus, this choice of scaling variable corresponds to assuming $b=-0.55$ in Eq. (70), which is significantly larger than what we find numerically. Therefore, if we use $(\beta_c^2 - \beta^2)$ as approximate thermal scaling field, the analytic corrections—in this case they are proportional to $(\beta_c^2 - \beta^2)^2$—are more important than in the case in which u_t is simply approximated with $\beta_c - \beta$.

The extended-scaling scheme can also be applied to the analysis of the susceptibility. It amounts to consider the scaling *Ansatz*[29]

$$\chi(\beta, L) = \beta^{\eta-2}\xi^{2-\eta}C(\xi/L). \tag{88}$$

In Fig. 19 we show $\beta^{2-\eta}\chi\xi^{\eta-2}$ versus ξ/L for the $\pm J$ model at $p=0.5$. Scaling is better than that observed in the upper panel of Fig. 15. The scatter of the data points is significantly reduced, indicating that $\beta^{\eta-2}$ approximates the scaling-field term $\bar{u}_h^2$ better than a constant. However, the rescaled data are still far from the asymptotic curve (the dashed line) determined numerically above, indicating that the residual analytic scaling corrections are also in this case not negligible. This is better understood, by comparing the function $\tilde{u}_h$, as determined in the fits, with the approximation $(\beta/\beta_c)^{\eta/2-1}$, which follows from Eq. (88). As can be seen from Fig. 17, the approximate expression proposed in Ref. 29 has the correct qualitative shape but differs significantly from the quantitative point of view. For these reasons, we do not expect scaling *Ansatz* (88) to be particularly useful in estimating η from our data.

To understand the role of the residual analytic scaling corrections on the determinations of η, we fit the data for the $\pm J$ model at $p=0.5$ to the scaling *Ansatz* (fit c)

$$\ln\frac{\chi\beta^2}{\xi^2} = -\eta \ln\frac{\xi}{\beta} + P_n(\xi/L), \tag{89}$$

where $P_n(x)$ is a polynomial of degree n. The results are reported in Fig. 19. They vary strongly with $\beta_{\min}$ and $L_{\min}$, indicating that scaling corrections are sizable and not negligible. As a test we have also repeated the fits to Eqs. (80) and (81) replacing $\ln \chi/\xi^2$ with $\ln \chi\beta^2/\xi^2$ and $\ln \xi$ with $\ln \xi/\beta$ [we call fit d and fit e the fits corresponding to Eqs. (80) and (81), respectively]. As expected, the results are identical to those obtained in fit b and fit c, respectively. Indeed, the fits only differ in the parametrization of the analytic function $\bar{u}_h$. Note that the extended-scaling approximation for $\bar{u}_h$ is not analytic in β since $\beta=0$ is a branching point. This is, however, irrelevant in practice since we are looking for approximations of $\bar{u}_h$ in the interval $0.6 \lesssim \beta \lesssim 0.9$, which is quite far from $\beta=0$.

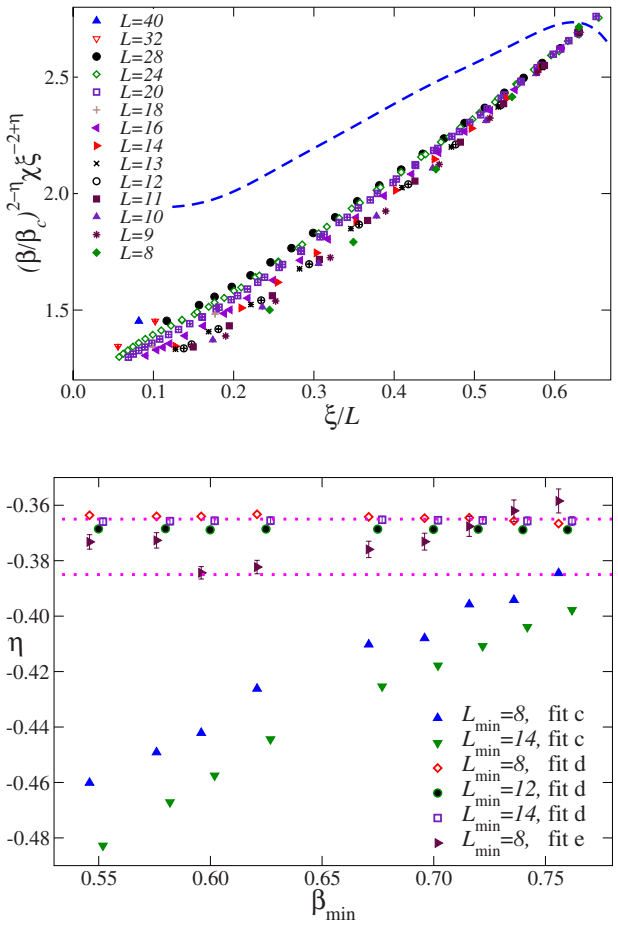

FIG. 19. (Color online) Extended-scaling results for the $\pm J$ model at $p=0.5$. In the upper panel we report $\beta^{2-\eta}\chi\xi^{\eta-2}$ vs ξ/L. The dashed line is the universal curve $\tilde{C}(\xi/L)$, as estimated in fits of χ to Eq. (80). In the lower panel we report estimates of η obtained in three different fits for several values of $L_{\min}$ and $\beta_{\min}$. Fit c uses *Ansatz* (89) and fits d and e are defined in text below Eq. (89). The dotted lines correspond to the estimate $\eta=-0.375(10)$.

VIII. ZERO-MOMENTUM QUARTIC COUPLINGS G_4 AND G_{22} IN THE HIGH-TEMPERATURE PHASE

In this section we consider the zero-momentum quartic couplings G_4 and G_{22} defined in Eqs. (19) and (20) and estimate their infinite-volume critical value defined by

$$G_{\#}^* = \lim_{\beta \to \beta_c^-} \lim_{L \to \infty} G_{\#}(L, \beta). \tag{90}$$

G_4^* and G_{22}^* are universal quantities, and therefore their values characterize the three-dimensional Ising spin glass universality class.

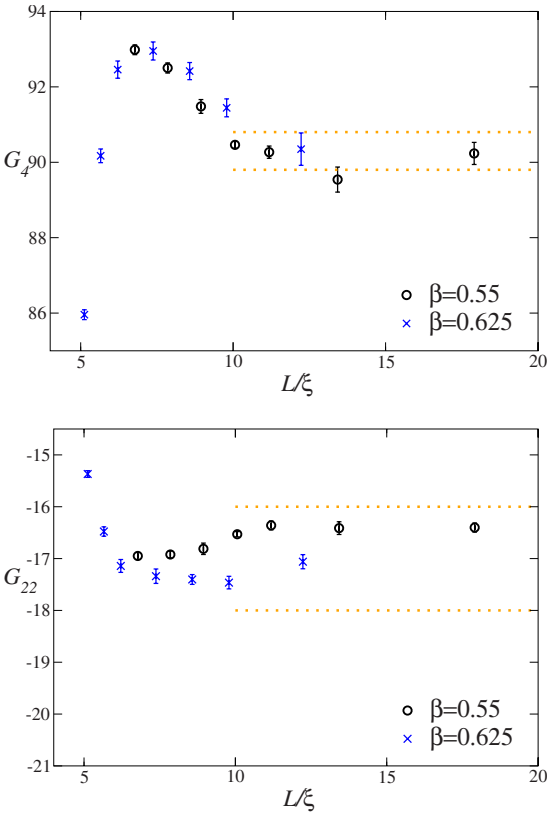

FIG. 20. (Color online) Estimates of $G_4(L,\beta)$ (top) and of $G_{22}(L,\beta)$ (bottom) versus L/ξ for $\beta=0.55$ and $\beta=0.625$, corresponding to the infinite-volume correlation lengths $\xi_\infty \approx 1.79$ and $\xi_\infty \approx 3.27$. Results for the $\pm J$ model at $p=0.5$. The dotted lines correspond to the estimates $G_4^*=90.3(5)$ (lower panel) and $G_{22}^*=-17(1)$ (lower panel).

We consider the $\pm J$ Ising model at $p=0.5$ and use the estimates of the quartic couplings for $\beta=0.55$ and $L=12$, 14, 16, 18, and 32 and for $\beta=0.625$ and $L=16$, 18, 28, 32, and 40. We combine results obtained in the random-exchange runs that we performed for our FSS study around β_c and results obtained in standard MC simulations for these two values of β.[76] First, we investigate the infinite-volume limit. The correlation length converges rapidly. For instance, for $\beta=0.55$ we obtain $\xi=1.7888(3), 1.7885(5), 1.7872(3)$ for $L=18, 20, 32$, while for $\beta=0.625$ we have $\xi=3.2694(12), 3.2709(13)$ for $L=32$ and $L=40$. For $L/\xi \gtrsim 10$ the results vary by less than 0.1%, indicating that the difference from their thermodynamic limit is within 0.1%. Thus, we can take as infinite-volume estimates those obtained on the largest lattices. The quartic couplings show larger finite-size corrections. As shown in Fig. 20 the infinite-volume limit is approximately reached for $L/\xi \gtrsim 12$, within our statistical precision. Indeed at $\beta=0.625$ we find $G_4=90.46(9)$, 90.27(16), and 90.23(29) and $G_{22}=-16.53(5)$, $-16.36(9)$, and $-16.40(9)$ for $L=18$, 20, and 32, respectively. We can thus take the estimates on the largest lattices as infinite-volume estimates.

In the critical limit we expect

$$G_\#(L=\infty,\beta) = G_\#^* + c_\# \xi^{-\omega} \tag{91}$$

with $\omega=1.0(1)$. The comparison of the results at $\beta=0.55$ and $\beta=0.625$ leads us to the estimates

$$G_4^* = 90.3(5), \quad G_{22}^* = -17(1), \tag{92}$$

where the error takes also into account the effects of the $O(\xi^{-\omega})$ scaling corrections, which are roughly estimated from the difference of the infinite-volume results at the two values of β.

The only available results for the zero-momentum quartic couplings $G_\#^*$ have been obtained for the random-anisotropy Heisenberg model in the limit of infinite anisotropy, whose critical behavior has been shown to belong to the Ising spin glass universality class.[27,36] The critical exponents were estimated in Ref. 27 by MC simulations, obtaining $\nu=2.4(6)$, $\eta=-0.24(4)$, and $\omega=1.0(4)$, which are substantially consistent with the Ising spin glass results obtained here. For the renormalized couplings, Ref. 27 obtained $G_4^*=88(8)$ and $G_{22}^*=-11(4)$, which are also in substantial agreement with estimates (92) within the quoted errors.

IX. CONCLUSIONS

In this paper we discuss the critical behavior of three-dimensional Ising spin glass systems with the purpose of verifying universality, clarifying the role of scaling corrections, and determining the critical exponents. More precisely, our results can be summarized as follows:

(i) By using the RG we derive the behavior for $L\to\infty$ and $\beta\to\beta_c$ of several quantities which are routinely measured in MC simulations. In particular, we show that the analytic dependence of the scaling fields on the model parameters may give rise to corrections which behave as $L^{-1/\nu}\sim L^{-0.4}$. If they are neglected, FSS analyses give inconsistent results. These corrections have been overlooked in previous FSS studies. Note that the general expressions we obtain are relevant also in other glassy systems, in which ν is typically large.

(ii) We determine the leading nonanalytic correction-to-scaling exponent ω. We obtain $\omega=1.0(1)$. Note that in Ising spin glass systems nonanalytic scaling corrections decay faster than in the Ising model, in which $\omega \approx 0.8$ (see Ref. 48). The exponent ω is also significantly larger than that at the PF transition, which occurs for small frustration: $\omega=0.29(2)$.[77]

(iii) We accurately verify universality. A careful analysis of U_4 and U_{22} at fixed $R_\xi=0.63$ shows that their limit for $L\to\infty$ is independent of the model and of the disorder distribution. The results obtained in the different models differ at most by approximately 1‰ in the case of $\bar{U}_4$ and 1% for $\bar{U}_{22}$. They support the existence of a unique Ising spin glass universality class. Universality is also supported by the FSS analyses of ξ and χ in the high-temperature phase. We verify that the FSS curves for these two quantities are independent of the model.

(iv) We determine the critical exponents. For this purpose we perform analyses at the critical point and analyses which take into account all high-temperature data. Results are consistent once the analytic and the nonanalytic corrections are taken into account. Moreover, they do not depend on the

model and disorder distribution. Again, this supports the universality of the paramagnetic-glassy transition. We obtain

$$\nu = 2.45(15), \quad \eta = -0.375(10). \tag{93}$$

Using scaling and hyperscaling relations, we find $\beta = \nu(1+\eta)/2 = 0.77(5)$, $\gamma = (2-\eta)\nu = 5.8(4)$, and $\alpha = 2-3\nu = -5.4(5)$.

Our estimates of the critical exponents can be compared with those reported in the literature. Earlier estimates of ν are reported in Sec. I and in Table I of Ref. 30. Some of the most recent ones are close to our final estimate. For the exponent η, we quote here the most recent results: $\eta = -0.395(17)$, $\eta = -0.37(5)$,[30] $\eta = -0.40(4)$,[29] and $\eta = -0.349(18)$.[28] They are all in substantial agreement with our result, which is however significantly more precise. We also mention the estimate $\beta = 0.52(9)$ obtained in Ref. 26 by an out-of-equilibrium simulation.

Estimates (93) slightly differ from, and have larger errors than, those obtained in Ref. 32: $\nu = 2.53(8)$ and $\eta = -0.384(9)$. There are two reasons for that. First, we have significantly extended the runs for $L = 20, 24$ for the $\pm J$ model at $p = 0.5$. The present results have slightly shifted the estimates of β_c and R_ξ^* and of the critical exponents. Second, we have been more conservative. With our present error bars, the estimates are fully consistent with the results of all analyses for the three models we considered.

We also analyzed our data by using the extended-scaling scheme proposed in Ref. 29. This approach might partly take into account the scaling corrections arising from the analytic dependence of the scaling fields on the reduced temperature but it neglects the nonanalytic corrections arising from the irrelevant operators. In some cases, for instance, for the overlap susceptibility, this scheme shows an apparent improvement of the scaling behavior with respect to the naive approach in which the analytic corrections are simply neglected. However, the approximate expressions which follow from the extended-scaling scheme are not sufficiently precise for a high-precision study of the critical behavior. If one aims at accurate estimates, it is necessary to determine the corrections directly from the data.

APPENDIX A: FINITE-SIZE BEHAVIOR OF THE PHENOMENOLOGICAL COUPLINGS

We now provide a detailed proof of Eq. (30) for the phenomenological couplings U_4, U_{22}, and $R_\xi \equiv \xi/L$. We start from the usual Wegner's scaling expression for the free energy.[37] We first consider U_4. Using Eq. (26), we find

$$[\mu_4] = L^d \frac{\partial^4 \mathcal{F}}{\partial h^4}\bigg|_{h=0} = L^{4y_h} \bar{u}_h^{-4} f^{(4)}(0, u_t L^{y_t}) + \cdots, \tag{A1}$$

$$[\mu_2] = L^d \frac{\partial^2 \mathcal{F}}{\partial h^2}\bigg|_{h=0} = L^{2y_h} \bar{u}_h^{-2} f^{(2)}(0, u_t L^{y_t}) + \cdots \tag{A2}$$

[the dots correspond to nonanalytic scaling corrections and bulk contributions and the derivatives refer to the first variable appearing in the scaling function $f(x,y)$], so that

$$U_4 = \frac{f^{(4)}(0, u_t L^{y_t})}{f^{(2)}(0, u_t L^{y_t})^2} + \cdots, \tag{A3}$$

which proves Eq. (30).

To discuss U_{22} one should generalize Wegner's scaling expression (see Sec. 3.1 of Ref. 47 for a detailed discussion). Define $Z(\beta, h, L)$ as the partition function of two systems at inverse temperature β defined on a lattice of size L^3 coupled by an interaction

$$h \sum_x \sigma_{1x} \sigma_{2x}. \tag{A4}$$

Then, consider

$$\mathcal{F}(\beta, h_1, h_2, L) = L^{-d} [\ln Z(\beta, h_1, L) \ln Z(\beta, h_2, L)]. \tag{A5}$$

A scaling *Ansatz* such as Eq. (25) allows one to obtain an expression analogous to that obtained for U_4 and to prove Eq. (30) for U_{22}.

In order to determine the scaling behavior of R_ξ we consider a momentum-dependent magnetic field. The argument goes as follows. Define $Z(\beta, h, L, p)$ as the partition function of two systems at inverse temperature β defined on a lattice of size L^3 coupled by an interaction $h \Sigma_x \sigma_{1x} \sigma_{2x} \cos(p \cdot x)$. Then, consider the corresponding disorder-averaged free-energy density

$$\mathcal{F}(\beta, h, L, p) = L^{-d} [\ln Z(\beta, h, L, p)]. \tag{A6}$$

Under RG transformations $L \to \lambda L$, momenta scale as $p \to p/\lambda$, so that the singular part of the free-energy density scales as

$$\mathcal{F}_{\rm sing}(\beta, h, L, p) = L^{-d} f(pL, u_h(h,t,p) L^{y_h}, u_t(h,t,p) L^{y_t}), \tag{A7}$$

where we have neglected the nonanalytic scaling corrections and now the scaling fields depend also on p. Taking derivatives with respect to h and then setting $h = 0$, we obtain for the two-point function [of course $u_h(h,t,-p) = u_h(h,t,p)$]

$$\tilde{G}(p) = \bar{u}_h(t,p)^2 L^{2-\eta} f^{(2)}(pL, 0, u_t(0,t,p) L^{y_t}), \tag{A8}$$

where we write as before

$$u_h(h,t,p) = h \bar{u}_h(t,p) + O(h^3), \tag{A9}$$

and we have neglected subleading terms. For $p \to 0$, because of the cubic symmetry of the lattice, we have

$$\bar{u}_h(t,p) = \bar{u}_h(t) + O(p^2), \tag{A10}$$

$$u_t(0,t,p) = u_t(0,t) + O(p^2), \tag{A11}$$

where $\bar{u}_h(t)$ and $u_t(0,t)$ are the usual (zero-momentum) scaling fields. Hence, for $p \to 0$, disregarding corrections of the order p^2, we can express $\tilde{G}(p)$ in terms of the scaling fields that appear for $p = 0$ as follows:

$$\tilde{G}(p) = \bar{u}_h(t)^2 L^{2-\eta} f^{(2)}(pL, 0, u_t(0,t)L^{y_t}) + O(p^2) + \cdots . \tag{A12}$$

In definition (14) of the correlation length ξ we should consider $p=q\sim 1/L$. Thus, disregarding terms of the order L^{-2} we have

$$\frac{\tilde{G}(0)-\tilde{G}(p)}{\tilde{G}(p)} = \frac{f^{(2)}(0,0,u_t(0,t)L^{y_t})}{f^{(2)}((2\pi,0,0),0,u_t(0,t)L^{y_t})} - 1$$
$$= \Phi(u_t(0,t)L^{y_t}). \tag{A13}$$

Neglecting again corrections of the order $1/L^2$, we have

$$\frac{\xi^2}{L^2} = \frac{1}{4\pi^2}\Phi(u_t(0,t)L^{y_t}), \tag{A14}$$

which proves Eq. (30). If we consider the corrections to scaling, this derivation shows that R_ξ behaves essentially as U_{22} and U_4. The only difference is the presence of corrections due to the momentum dependence of the scaling fields and to the specific definition of the correlation length. They scale as $L^{-2}, L^{-4}, \ldots, L^{-\omega-2}, \ldots$. Since $\omega \approx 1$, in Eq. (30) they represent additional subleading corrections and can thus be neglected. This allows us to consider R_ξ, U_{22}, and U_4 on the same footing.

APPENDIX B: SOME TECHNICAL DETAILS ON THE MC SIMULATIONS

In our MC simulations we implement the standard METROPOLIS algorithm with a sequential update of the spins. We use a multispin[78] implementation, in which $n_{\rm bit}=64$ systems are simulated in parallel. For each of them we use a different set of bonds $\{J_{xy}\}$.

For the random numbers we use the SIMD-oriented (SIMD is the usual acronym for "single-instruction multiple-data") fast Mersenne twister (SFMT) (Ref. 79) generator. In particular, we use the *genrand-res53()* function that produces double-precision output. Independent random numbers are employed to generate the starting configurations for each disorder realization and in the parallel-tempering updates. In the latter case very few random numbers are used; thus, it takes virtually no extra time to use individual random numbers for each of the $n_{\rm bit}$ systems which are simulated in parallel. On the other hand, in order to save CPU time, we use the same sequence of random numbers for the local METROPOLIS update of any of the $n_{\rm bit}$ systems. Although this choice does not lead to wrong estimates of the expectation values, it might create a statistical correlation among the $n_{\rm bit}$ systems. However, since each of the $n_{\rm bit}$ systems corresponds to a different set of bond couplings J_{xy} we expect this effect to be negligible. Nevertheless, in order to ensure a correct estimate of the statistical error, in our jackknife analysis we put all $n_{\rm bit}$ systems that use the same sequence of random numbers in the same bin. In order to compute overlap observables, we performed runs for two systems with the same set $\{J_{xy}\}$ in parallel. In our MC simulations a single METROPOLIS update of a single spin takes about 1.2×10^{-9} s on an Opteron CPU running at 2 GHz (this should be compared with the speed of the dedicated computer Janus,[33] the fastest computer simulating discrete spin models, which takes 2×10^{-11} s to update an Ising spin).

To reduce autocorrelations we used the random-exchange or parallel-tempering method.[69] To this end, we divided the interval $[\beta_{\rm min}, \beta_{\rm max}]$ into $N_\beta - 1$ equal intervals $\Delta\beta$. The parameter $\beta_{\rm max}$ was chosen such that $\xi(\beta_{\rm max})/L \approx 0.63$ in most cases; in the latest runs we considered larger values such that $\xi(\beta_{\rm max})/L \approx 0.66$. The parameter $\beta_{\rm min}$ was chosen such that $\xi(\beta_{\rm min}) \ll L$. We computed the observables in the neighborhood of $\beta_{\rm max}$ by using their second-order Taylor expansion around $\beta_{\rm max}$. The coefficients of the expansion can be written as expectation values of products of the observables and powers of the energy, which were measured in the simulation.

An elementary update unit consists of $n_{\rm met}$ METROPOLIS sweeps followed by a replica exchange of all pairs of systems at nearby temperatures. The different systems were sequentially visited, starting from those at $\beta_{\rm min}$ and $\beta_{\rm min}+\Delta\beta$. As a candidate for the exchange, we considered one of two replicas with equal probabilities. The acceptance probability for the exchange is $\min[1, \exp(-\Delta\beta\Delta H)]$. Since the measurement of the energy in our implementation costs more CPU time than a METROPOLIS sweep, we chose $n_{\rm met} \gg 1$ independent of β.

The computation of disorder averages of products of thermal expectations requires particular care. Indeed, naive estimators have a bias which may become larger than statistical errors.[70] To avoid the problem we consider essentially bias-free estimators, defined following Ref. 47. For this purpose we divide the measurement phase of the run into 12 intervals. Between each pair of subsequent intervals there is a decorrelation phase. In total, the run consists of the following phases: $Eq, D_1 M_1, D_2 M_2, \ldots, D_{12} M_{12}$. After some tests, we fixed the number of update steps for each of them. The equilibration phase Eq corresponds to $20 n_{\rm temp}$ elementary update units; the measurement phases M_i correspond to $n_{\rm temp}$ update units, while the length of D_i is $n_{\rm temp}$ for $i\neq 7$ and $5n_{\rm temp}$ for $i=7$. Recall that each elementary update unit corresponds to $n_{\rm met}$ METROPOLIS sweeps of all systems and to one full tempering sweep.

The presence of different measurement phases allows us to define bias-free quantities. To define $[\langle A\rangle\langle B\rangle]$ (for instance, this is relevant for the computation of U_{22}) we average over the samples the quantity

$$\frac{1}{2\times 6\times 6}\sum_{i=1}^{6}\sum_{j=7}^{12}[\mu(A)_i\mu(B)_j + \mu(A)_j\mu(B)_i], \tag{B1}$$

where $\mu(A)_i$ is the average of the estimates of A obtained in the measurement phase M_i. Analogously, to compute $[\langle A\rangle\langle B\rangle\langle C\rangle]$ (these correlators are necessary to compute the coefficients of the Taylor expansions around a given value of β), we average over the samples the quantity

$$\frac{1}{3!\times 4^3}\sum_{i=1}^{4}\sum_{j=5}^{8}\sum_{k=9}^{12}[\mu(A)_i\mu(B)_j\mu(C)_k + 5 \text{ permutations}]. \tag{B2}$$

In order to check equilibration and decorrelation for the bias correction, we followed the suggestion of Ref. 30. We

TABLE IV. Summary of the parameters for the runs at $p=0.5$. N_β is the number of β values used in the parallel-tempering simulation. The rest of the notation is explained in the text. The CPU time refers to a single core of a dual core Opteron CPU running at 2.4 GHz.

L	Samples/64	n_{met}	n_{temp}	N_β	β_{min}	β_{max}	CPU time (days)
4	100000	5	40	5	0.58	0.92	
5	100000	5	50	5	0.58	0.908	
6	100000	5	50	5	0.58	0.9018	1
7	119103	5	80	5	0.58	0.899	3
8	100000	5	80	5	0.58	0.8975	4
9	110850	10	100	8	0.55	0.8962	27
10	100681	10	150	8	0.55	0.896	50
11	109779	10	300	10	0.54	0.8955	183
12	106812	10	400	10	0.54	0.8955	308
13	38282	10	600	10	0.54	0.8955	210
14	31600	50	200	10	0.62	0.8955	361
16	24331	10	1000	20	0.52	0.895	830
20	1542	20	2000	32	0.5125	0.895	658
20	2291	50	1500	20	0.625	0.91	1146
24	717	25	2500	32	0.5125	0.895	826
24	1627	50	2000	20	0.625	0.91	1874
28	285	60	2500	20	0.6575	0.895	782

doubled the length of the run until the estimates of all observables were consistent within error bars. We performed this check only for the observables at β_{max} because these are expected to be the most difficult ones for equilibration and decorrelation. Starting from disordered configurations, we determined the number of update steps n_{half} that are needed to reach (averaged over samples) half of the equilibrium value of the overlap susceptibility. In total, the equilibration consisted of at least $100n_{\mathrm{half}}$ update steps. Using these methods to check equilibration, we came up with the choices summarized in Table IV. The parameters are not highly tuned since we had the CPU time available on short notice. The runs that were done later have typically a larger β_{min} than those done earlier. The run for $L=28$ is a bit at the edge of the criterion given above for equilibration. However, given the rather small number of samples ($N_s=18\,240$), we are quite confident that the estimates are correct within the quoted error bars.

[1] S. F. Edwards and P. W. Anderson, J. Phys. F **5**, 965 (1975).
[2] A. Ito, H. Aruga, E. Torikai, M. Kikuchi, Y. Syono, and H. Takei, Phys. Rev. Lett. **57**, 483 (1986).
[3] K. Gunnarsson, P. Svedlindh, P. Nordblad, L. Lundgren, H. Aruga, and A. Ito, Phys. Rev. B **43**, 8199 (1991).
[4] S. Nair and A. K. Nigam, Phys. Rev. B **75**, 214415 (2007).
[5] A. T. Ogielski and I. Morgenstern, Phys. Rev. Lett. **54**, 928 (1985).
[6] A. T. Ogielski, Phys. Rev. B **32**, 7384 (1985).
[7] W. L. McMillan, Phys. Rev. B **31**, 340 (1985).
[8] A. J. Bray and M. A. Moore, Phys. Rev. B **31**, 631 (1985).
[9] R. N. Bhatt and A. P. Young, Phys. Rev. Lett. **54**, 924 (1985).
[10] R. R. P. Singh and S. Chakravarty, Phys. Rev. Lett. **57**, 245 (1986).
[11] J. D. Reger and A. Zippelius, Phys. Rev. Lett. **57**, 3225 (1986).
[12] R. N. Bhatt and A. P. Young, Phys. Rev. B **37**, 5606 (1988).
[13] E. Marinari, G. Parisi, and F. Ritort, J. Phys. A **27**, 2687 (1994).
[14] N. Kawashima and A. P. Young, Phys. Rev. B **53**, R484 (1996).
[15] L. W. Bernardi, S. Prakash, and I. A. Campbell, Phys. Rev. Lett. **77**, 2798 (1996).
[16] D. Iñiguez, G. Parisi, and J. J. Ruiz-Lorenzo, J. Phys. A **29**, 4337 (1996).
[17] B. A. Berg and W. Janke, Phys. Rev. Lett. **80**, 4771 (1998).
[18] E. Marinari, G. Parisi, and J. J. Ruiz-Lorenzo, Phys. Rev. B **58**, 14852 (1998).
[19] P. O. Mari and I. A. Campbell, Phys. Rev. E **59**, 2653 (1999).
[20] M. Palassini and S. Caracciolo, Phys. Rev. Lett. **82**, 5128 (1999).
[21] H. G. Ballesteros, A. Cruz, L. A. Fernández, V. Martín-Mayor, J. Pech, J. J. Ruiz-Lorenzo, A. Tarancón, P. Téllez, C. L. Ullod, and C. Ungil, Phys. Rev. B **62**, 14237 (2000).
[22] P. O. Mari and I. A. Campbell, Phys. Rev. B **65**, 184409 (2002).
[23] T. Nakamura, S.-i. Endoh, and T. Yamamoto, J. Phys. A **36**, 10895 (2003).
[24] D. Daboul, I. Chang, and A. Aharony, Eur. Phys. J. B **41**, 231 (2004).
[25] M. Pleimling and I. A. Campbell, Phys. Rev. B **72**, 184429 (2005).

[26] S. Perez Gaviro, J. J. Ruiz-Lorenzo, and A. Tarancón, J. Phys. A **39**, 8567 (2006).
[27] F. Parisen Toldin, A. Pelissetto, and E. Vicari, J. Stat. Mech.: Theory Exp. (2006) P06002.
[28] T. Jörg, Phys. Rev. B **73**, 224431 (2006).
[29] I. A. Campbell, K. Hukushima, and H. Takayama, Phys. Rev. Lett. **97**, 117202 (2006).
[30] H. G. Katzgraber, M. Körner, and A. P. Young, Phys. Rev. B **73**, 224432 (2006).
[31] J. Machta, C. M. Newman, and D. L. Stein, J. Stat. Phys. **130**, 113 (2008); arXiv:0805.0794 (unpublished).
[32] M. Hasenbusch, A. Pelissetto, and E. Vicari, J. Stat. Mech.: Theory Exp. (2008) L02001.
[33] F. Belletti, M. Cotallo, A. Cruz, L. A. Fernández, A. Gordillo-Guerrero, M. Guidetti, A. Maiorano, F. Mantovani, E. Marinari, V. Martín-Mayor, A. Muñoz Sudupe, D. Navarro, G. Parisi, S. Perez-Gaviro, J. J. Ruiz-Lorenzo, S. F. Schifano, D. Sciretti, A. Tarancón, R. Tripiccione, J. L. Velasco, and D. Yllanes (the Janus Collaboration), Comput. Phys. Commun. **178**, 208 (2008).
[34] T. Jörg, H. G. Katzgraber, and F. Krzakała, Phys. Rev. Lett. **100**, 197202 (2008).
[35] K. H. Chen and T. C. Lubensky, Phys. Rev. B **16**, 2106 (1977).
[36] F. Liers, J. Lukic, E. Marinari, A. Pelissetto, and E. Vicari, Phys. Rev. B **76**, 174423 (2007).
[37] F. J. Wegner, in *Phase Transitions and Critical Phenomena*, edited by C. Domb and M. S. Green (Academic, New York, 1976), Vol. 6.
[38] I. A. Campbell, K. Hukushima, and H. Takayama, Phys. Rev. B **76**, 134421 (2007).
[39] H. Nishimori, Prog. Theor. Phys. **66**, 1169 (1981).
[40] A. Georges, D. Hansel, P. Le Doussal, and J. Bouchaud, J. Phys. (Paris) **46**, 1827 (1985).
[41] P. Le Doussal and A. B. Harris, Phys. Rev. Lett. **61**, 625 (1988); Phys. Rev. B **40**, 9249 (1989).
[42] H. Nishimori, *Statistical Physics of Spin Glasses and Information Processing: An Introduction* (Oxford University Press, Oxford, 2001).
[43] M. Hasenbusch, F. P. Toldin, A. Pelissetto, and E. Vicari, Phys. Rev. B **76**, 184202 (2007).
[44] Y. Deng and H. W. J. Blöte, Phys. Rev. E **68**, 036125 (2003).
[45] M. Hasenbusch, F. P. Toldin, A. Pelissetto, and E. Vicari, Phys. Rev. B **76**, 094402 (2007).
[46] M. Campostrini, A. Pelissetto, P. Rossi, and E. Vicari, Phys. Rev. E **65**, 066127 (2002).
[47] M. Hasenbusch, F. Parisen Toldin, A. Pelissetto, and E. Vicari, J. Stat. Mech.: Theory Exp. (2007) P02016.
[48] A. Pelissetto and E. Vicari, Phys. Rep. **368**, 549 (2002).
[49] G. Toulouse, J. Phys. Lett. **41**, 447 (1980).
[50] N. Kawashima and H. Rieger, in *Frustrated Spin Systems*, edited by H. T. Diep (World Scientific, Singapore, 2004); arXiv:cond-mat/0312432 (unpublished).
[51] H. Nishimori, J. Phys. Soc. Jpn. **55**, 3305 (1986).
[52] H. Kitatani, J. Phys. Soc. Jpn. **61**, 4049 (1992).
[53] C. Wang, J. Harrington, and J. Preskill, Ann. Phys. **303**, 31 (2003).
[54] C. Amoruso and A. K. Hartmann, Phys. Rev. B **70**, 134425 (2004).
[55] M. Picco, A. Honecker, and P. Pujol, J. Stat. Mech.: Theory Expt. (2006) P09006.
[56] A. K. Hartmann, Phys. Rev. B **59**, 3617 (1999).
[57] It can be shown rigorously that the Nishimori line never intersects the spin glass phase [H. Kitatani, J. Phys. Soc. Japan **63**, 2070 (1994)]. Since we must also have $p_{\rm FG} \leq p^*$, the mixed phase, if it exists, should be confined to the region below the Nishimori line and on the left of the line $p=p^*$ (see Fig. 1).
[58] D. Sherrington and S. Kirkpatrick, Phys. Rev. Lett. **35**, 1792 (1975).
[59] T. Castellani, F. Krzakala, and F. Ricci Tersenghi, Eur. Phys. J. B **47**, 99 (2005).
[60] F. Krzakala and O. C. Martin, Phys. Rev. Lett. **89**, 267202 (2002).
[61] S. Boettcher and E. Marchetti, Phys. Rev. B **77**, 100405(R) (2008).
[62] S. Boettcher and J. Davidheiser, Phys. Rev. B **77**, 214432 (2008).
[63] C. D. Lorenz and R. M. Ziff, Phys. Rev. E **57**, 230 (1998).
[64] T. Jörg and F. Ricci-Tersenghi, Phys. Rev. Lett. **100**, 177203 (2008).
[65] V. Privman, in *Finite Scaling and Numerical Simulations of Statistical Systems*, edited by V. Privman (World Scientific, Singapore, 1990).
[66] J. Salas and A. D. Sokal, J. Stat. Phys. **98**, 551 (2000).
[67] M. Campostrini, M. Hasenbusch, A. Pelissetto, and E. Vicari, Phys. Rev. B **74**, 144506 (2006).
[68] M. Hasenbusch, J. Phys. A **32**, 4851 (1999).
[69] C. J. Geyer, in *Computer Science and Statistics: Proceedings of the 23rd Symposium on the Interface*, edited by E. M. Keramidas (Interface Foundation, Fairfax Station, 1991), p. 156; K. Hukushima and K. Nemoto, J. Phys. Soc. Jpn. **65**, 1604 (1996); for a review, see D. J. Earl and M. W. Deem, Phys. Chem. Chem. Phys. **7**, 3910 (2005).
[70] H. G. Ballesteros, L. A. Fernández, V. Martín-Mayor, A. Muñoz Sudupe, G. Parisi, and J. J. Ruiz-Lorenzo, Nucl. Phys. B **512**, 681 (1998).
[71] See EPAPS Document No. E-PRBMDO-78-003845 for tables of Monte Carlo data. For more information on EPAPS, see http://www.aip.org/pubservs/epaps.html.
[72] In practice, we write $R(L,\beta)=R(L,\beta_{\rm run})+a_R(L)(\beta-\beta_{\rm run})+b_R(L)(\beta-\beta_{\rm run})^2$, where $\beta_{\rm run}$ is the value of β closest to β_c we have considered in the simulation (typically $\beta_{\rm run}=\beta_{\rm max}$; see Sec. IV) and $R(L,\beta_{\rm run})$, $a_R(L)$, and $b_R(L)$ are determined in the simulation. Then, β_c, b, and R^* are determined by minimizing the usual χ^2 variable.
[73] P. Calabrese, V. Martín-Mayor, A. Pelissetto, and E. Vicari, Phys. Rev. E **68**, 036136 (2003).
[74] In the fit we minimize $\Sigma_i[\Xi_i - P_n(x_i)]^2/\sigma_i^2$, where $\Xi=(\xi/L)^{-n/\nu}$, the sum is over all data points, $\sigma_i=(n/\nu)\Xi_i\Delta\xi_i/\xi_i$, and $\Delta\xi_i$ is the error on ξ_i. Errors are obtained by using a jackknife procedure and take into account the statistical correlations among the data. At fixed ν and β_c the fit is linear and the result is obtained by inverting the least-squares matrix. This matrix is ill conditioned (the condition number is of the order of 10^{24}–10^{32}, depending on n). This required the use of 128-digit arithmetic in the calculations.
[75] S. Caracciolo, R. G. Edwards, S. J. Ferreira, A. Pelissetto, and A. D. Sokal, Phys. Rev. Lett. **74**, 2969 (1995).
[76] The finite thermodynamic limit of G_{22} indicates that self-averaging holds in the high-temperature phase. Therefore, as the lattices become larger at a given temperature, it becomes convenient to improve the statistical accuracy of the expectation val-

ues for a given sample. To this end we simulate $n>2$ copies of the system with the same couplings J_{xy}. We compute the overlap from all $n(n-1)/2$ pairs.

[77] M. Hasenbusch, A. Pelissetto, and E. Vicari, J. Stat. Mech.: Theory Exp. (2007) P11009.

[78] See, e.g., S. Wansleben, J. B. Zabolitzky, and C. Kalle, J. Stat. Phys. **37**, 271 (1984); G. Bhanot, D. Duke, and R. Salvador, Phys. Rev. B **33**, 7841 (1986).

[79] The numerical program and a detailed description can be found at http://www.math.sci.hiroshima-u.ac.jp/~m-mat/MT/SFMT/index.html.